

# Near-Infrared Imaging of Barred Halo Dominated Low Surface Brightness Galaxies

M. Honey<sup>1,2\*</sup>, M. Das<sup>1†</sup>, J.P. Ninan<sup>3‡</sup>, M. Purvankara<sup>3§</sup>

<sup>1</sup>*Indian Institute of Astrophysics, Koramanagala, BangalorE-560034, India.*

<sup>2</sup>*Pondicherry University, R. Venkataraman Nagar, Kalapet, 605014 Pondicherry, India.*

<sup>3</sup>*Tata Institute of Fundamental Research, Mumbai 400005, India.*

Accepted 2016 June 22; Received 2016 June 19; in original form 2016 March 09

## ABSTRACT

We present a near-infrared (NIR) imaging study of barred low surface brightness (LSB) galaxies using the TIFR near-infrared Spectrometer and Imager (TIRSPEC). LSB galaxies are dark matter dominated, late type spirals that have low luminosity stellar disks but large neutral hydrogen (HI) gas disks. Using SDSS images of a very large sample of LSB galaxies derived from the literature, we found that the barred fraction is only 8.3%. We imaged twenty five barred LSB galaxies in the J, H,  $K_S$  wavebands and twenty nine in the  $K_S$  band. Most of the bars are much brighter than their stellar disks, which appear to be very diffuse. Our image analysis gives deprojected mean bar sizes of  $R_b/R_{25} = 0.40$  and ellipticities  $e \approx 0.45$ , which are similar to bars in high surface brightness galaxies. Thus, although bars are rare in LSB galaxies, they appear to be just as strong as bars found in normal galaxies. There is no correlation of  $R_b/R_{25}$  or  $e$  with the relative HI or stellar masses of the galaxies. In the (J- $K_S$ ) color images most of the bars have no significant color gradient which indicates that their stellar population is uniformly distributed and confirms that they have low dust content.

**Key words:** galaxies : spiral; galaxies: structure; galaxies: evolution; infrared : galaxies.

## 1 INTRODUCTION

Low Surface Brightness galaxies are extreme late type spiral galaxies that are optically dim and have a central disk surface brightness fainter than 22 magnitudes/arcsec<sup>2</sup> in the B band (Impey & Bothun 1997). They have diffuse stellar disks, that are low in metallicity (McGaugh 1994) and dust content (Rahman et al. 2007; Hinz et al. 2007). They are rich in neutral hydrogen (HI) gas (O’Neil et al. 2004) but have low star formation rates (Boissier et al. 2008; O’Neil et al. 2004). They can be broadly classified into LSB spirals and LSB dwarf or irregular galaxies. Of the LSB spirals, a significant fraction have very large disks and HI gas masses; these galaxies are often referred to as giant LSB (GLSB) galaxies of which UGC 6614, Malin 1 and Malin 2 are very good examples (Pickering et al. 1997; Sprayberry et al. 1995). GLSB galaxies are usually seen in isolated environments (Rosenbaum et al. 2009) but the smaller LSB dwarf and irregu-

lar galaxies are found in both underdense regions (Pustilnik et al. 2011) as well as more crowded environments (Merritt, van Dokkum & Abraham 2014; Javanmardi et al. 2016; Davies, Davies & Keenan 2016).

One of the distinguishing features of LSB galaxies is their very large dark matter content (de Blok et al. 2001). Their dominant dark matter halos suppresses the formation of both global and local disk instabilities (Mihos, McGaugh & de Blok 1997) thus hampering the formation of bars and strong spiral arms in these galaxies (Mayer & Wadsley 2004). Thus it is not surprising that bars are relatively rare in LSB galaxies and spiral arms are thin compared to those found in high surface brightness (HSB) galaxies. However, although barred LSB galaxies are rare, they are the best systems in which to understand the formation and evolution of bars in dark matter dominated disks. Although there have been many simulation studies of bars in halo dominated disks (Long, Shlosman & Heller 2014; Saha & Naab 2013a; Villa-Vargas, Shlosman & Heller 2010), there are surprisingly no near-infrared (NIR) or optical studies of bars in halo dominated disk galaxies. One of the main aims of this paper is to

\* E-mail : mhoney@iiap.res.in

† E-mail : mousumi@iiap.res.in (MD)

‡ E-mail : ninan@tifr.res.in)

§ E-mail : manoj.purvankara@tifr.res.in)

provide a deep NIR study of bars in LSB galaxies and see how they differ from normal bright galaxies.

Bars play an important role in disk evolution through several dynamical effects. First, they drive gas into the centers of galaxies resulting in the buildup of central mass concentrations that can lead to bulge growth (Norman, Sellwood & Hasan 1996; Bournaud, Combes & Semelin 2005; Fanali et al. 2015) as well as disk star formation (Ellison et al. 2011). During this process, gas may collect at the resonance radii in the disks - such as the corotation radii at the bar ends, circumnuclear rings within the bars or at resonance radii in the outer disks (Sellwood & Wilkinson 1993). If the gas surface density in these rings is large enough, local instabilities can result in the formation of bright star forming rings at the resonance radii (Buta 1986). Such rings are clearly seen in the larger LSB galaxies such as UGC 6614 (Mapelli & Moore 2008). Secondly, bars can themselves also evolve into rounder bars or boxy bulges in disks. This change in bar morphology can occur rapidly due to bending instabilities in bars (Raha et al. 1991) or alternatively there may be a slow dissolution of the bar structure caused by gas infall and the buildup of a central mass concentration (Das et al. 2003; Das et al. 2008). This slow internal evolution of bars is often referred to as the secular evolution of barred galaxies (Kormendy & Kennicutt 2004; Combes et al. 1990; Combes & Sanders 1981; Sheth et al. 2005). LSB galaxies are usually isolated and are hence ideal systems in which to study secular evolution of bars into boxier bulges. As our study shows, LSB bulges are not always classical bulges; a definite indication that bulges evolve even in the most isolated environments.

In this paper we present near infrared (NIR) imaging in the J, H,  $K_S$  bands of a sample of barred LSB galaxies using the TIFR NIR Spectrometer and Imager (TIRSPEC) that is mounted on the Himalayan Chandra Telescope (HCT). Our aim is to study bar morphologies in LSB galaxies; their sizes, shapes, colors and correlation with other galaxy properties such as stellar and HI gas masses. We have also examined the  $K_S$  band isophotes for signatures of bar evolution (boxy shapes), interactions or nested bars (twisted isophotes). In the following sections we describe our sample selection and our estimate of bar fraction in LSB galaxies. We then describe our observations, results and discuss the implications of our study.

## 2 SAMPLE SELECTION

Observational studies show that about one third of all disk galaxies are barred (Simmons et al. 2014; Menéndez-Delmestre et al. 2007; Marinova & Jogee 2007). To see if the fraction of bars is different for LSB galaxies we have visually examined the Sloan Digital Sky Survey (SDSS) images of a sample of 938 LSB galaxies that were collected from catalogues in the literature (Impey et al. 1996; Schombert & Bothun 1988; Schombert et al. 1992; Schombert 1998). However, only 854 galaxies had SDSS images. We visually examined the SDSS (Data Release12) images of these galaxies and found that 69 are barred. We had previous HCT observations of two more LSB galaxies UGC 2936 and UGC 11754 that are not covered in SDSS, but were clearly

barred. This gives the barred fraction of LSB galaxies to be 71/856 or 8.3%. However, we had taken those galaxies which are brighter enough to observe with TIRSPEC and excluded the very faint galaxies, since they are extremely difficult to image in NIR. We were also limited by sky conditions during our observations. Hence we were able to observe a total of 29 barred LSB galaxies. Of these, 25 were covered in the J, H and  $K_S$  bands. The galaxies LSBC F570-01, IC 2423, 1442+0137 and LSBC F675-01 have only  $K_S$  band images. The sample details are given in Table 1.

## 3 OBSERVATIONS

Our NIR and optical observations were done with the near-IR imager TIRSPEC which is mounted on the 2m Himalayan Chandra Telescope (HCT), which is part of the Indian Astronomical Observatory in Hanle in the Himalayas. The telescope is remotely operated from Centre for Research and Education in Science and Technology (CREST), Bangalore. TIRSPEC is a medium resolution NIR spectrometer and imager covering a wavelength range of 1 to 2.5  $\mu m$ . It has a field of view of  $307 \times 307$  arcsec<sup>2</sup> and a plate scale of 0.3 arcsec pixel<sup>-1</sup>. The observations were done over the period August 2014 to May 2015. We have taken the images in J, H and  $K_S$  broad band filters. In each of the filters we have done a minimum of five dither positions and each dither position has three to twenty frames of 15 to 20 second exposures each according to the brightness of the galaxy. Besides the target frames, the sky frames were also taken in J, H and  $K_S$  bands immediately after the target frames in the different dither positions with at least three frames in each position. The dark frames, twilight flats and morning flats were used for preprocessing the images. The observation details are given in Table 2.

For two galaxies, UGC 11754 and UM 163, we had to do separate R band observations in order to determine the position angle (PA) or major axis of the galaxy which is required for estimating the deprojected bar lengths and ellipticities. UGC 11754 is not covered in the SDSS and the galaxy UM 163 is on the edge of the frame, which made it difficult to obtain the position angle of the disk. Although we did obtain NIR images of these galaxies, it was extremely difficult to image the faint, diffuse outer parts of the stellar disks which are needed to derive the position angle of the galaxy. So we have carried out the optical R-band observation for these two galaxies with the Himalayan Faint Object Spectrograph Camera (HFOSC), that has a plate scale of 0.296 arcsec pixel<sup>-1</sup>, and has a field of view of  $10 \times 10$  arcmin<sup>2</sup>. The details of optical observations are given in Table 3.

## 4 DATA REDUCTION

The NIR data reduction was carried out using the TIRSPEC semi automated reduction pipeline (Ninan et al. 2014) written in python, that allows the visual inspection of individ-

**Table 1.** The barred LSB galaxies. The D<sub>25</sub> is the physical major axis of the galaxy at the 25 mag/arcsec<sup>2</sup> in B band

Galaxy name	RA & DEC (J 2000)	Redshift	morphology (NED)	D <sub>25</sub> (arcsec)	scale (kpc/arcsec)	D <sub>25</sub> (kpc)	Active
CGCG 381-048	23h47m21.1s +01d56m01s	0.0176	SBc	***	0.319	***	**
UGC 1920	02h27m51.8s +45d56m49s	0.0207	(R')SB(s)ab	90.8	0.389	35.32	**
UGC 1455	01h58m48.0s +24d53m33s	0.0171	SAB(rs)bc	165.30	0.316	52.23	**
NGC 5905	15h15m23.3s +55d31m03s	0.0113	SB(r)b	238.90	0.226	53.99	yes-Sy1
UM163	23h30m32.3s -02d27m45s	0.0334	SB(r)b pec	111.7	0.617	68.92	yes-Sy1.2
UGC 11754	21h29m31.5s +27d19m17s	0.0161	SABcd	106.70	0.294	31.37	**
PGC 68495	22h17m13.1s +25d12m48s	0.0422	SBc(r)	52.30	0.779	40.74	**
UGC 2936	04h02m48.2s +01d57m58s	0.0127	SB(s)d	150.70	0.242	36.47	yes-Sy2
UGC 10405	16h28m54.1s +17d53m27s	0.0363	Scd	95.10	0.695	66.09	**
0223-0033	02h26m06.7s -00d19m55s	0.0214	SB(rs)bc	109.20	0.400	43.68	yes-LINER
UGC 5035	09h27m10.2s +21d35m38s	0.0370	(R)SB(s)a	65.80	0.722	47.50	**
UGC 09087	14h12m16.8s +18d17m58s	0.0171	S0	70.50	0.349	24.60	**
LSBC F568-08	10h34m08.7s +19d42m15s	0.0341	Sb	57.09 (SDSS-r)	0.671	38.30	**
LSBC F568-09	10h28m12.0s +18d36m23s	0.0269	SBc-p-	44.30 (SDSS-r)	0.539	23.88	**
UGC 9634	14h58m57.9s +20d03m10s	0.0428	SB(s)b	62.80	0.820	51.50	**
IC 742	11h51m02.2s +20d47m59s	0.0214	SBab	65.8	0.436	28.69	**
UGC 8794	13h52m57.7s +20d55m01s	0.0286	Sb	73.8	0.566	41.77	**
UGC 9927	15h36m27.8s +22d30m02s	0.0144	SB0	54.7	0.290	15.86	**
LSBC F584-01	16h05m36.8s +22d11m11s	0.0401	S	52.3	0.766	40.06	**
LSBC F580-02	14h36m44.7s +21d04m22s	0.0181	Sc(r)	**	**	**	**
UGC 3968	07h42m45.2s +66d15m30s	0.0226	SB(r)c	84.8	0.441	37.40	**
1300+0144	13h03m16.0s +01d28m07s	0.0409	Sc(f)	60.52(SDSS-r)	0.795	48.11	**
PGC 60365	17h28m54.6s +25d49m03s	**	SBb	**	**	**	**
CGCG 006-023	09h16m13.7s +00d42m02s	0.0381	Sbc	50.55 (SDSS-r)	0.746	37.71	**
1252+0230	12h55m25.9s +02d13m52s	0.0480	Sc	44.64 (SDSS-r)	0.922	41.16	**
LSBC F570-01	11h17m57.9s +22d30m11s	0.0259	SB0	69.27 (SDSS-r)	0.521	36.08	**
1442+0137	14h45m00.2s +01d24m31s	0.0338	Sc	32.42(SDSS-r)	0.661	21.43	**
LSBC F675-01	22h40m35.3s +13d58m38s	0.0368	S/ring	25.55(SDSS-r)	0.678	17.32	**
IC 2423	08h54m47.1s +20d13m13s	0.0305	SAB(s)b	62.8 (SDSS-r)	0.6	37.68	**

**Table 2.** The Ks band observations of the sample galaxies.

Galaxy	date	number of dither positions	number of frames per dither position	Frame exposure (s)	Total exposure time (s)
CGCG 381-048	22-08-2014	5	3	20	300
UGC 1920	29-08-2014	5	3	20	300
UGC 1455	29-08-2014	5	6	15	450
UGC 5905	17-09-2014	5	6	15	450
UM 163	17-09-2014	5	6	20	600
UGC 11754	23-09-2014	5	10	30	1500
PGC 68495	23-09-2014	5	6	20	600
UGC 2936	23-09-2014	5	6	20	600
UGC 10405	12-10-2014	5	6	20	600
0223-0033	10-11-2014	5	6	20	600
UGC 5035	10-11-2014	5	6	20	600
UGC 9087	02-12-2014	5	6	20	600
LSBC F568-08	09-12-2014	5	6	20	600
LSBC F568-09	09-01-2015	5	10	20	1000
UGC 9634	20-03-2015	7	10	20	1400
IC 742	18-05-2015	5	10	20	1000
UGC 8794	18-05-2015	5	10	20	1000
UGC 9927	18-05-2015	5	10	20	1000
LSBC F584-01	28-05-2015	5	20	20	2000
LSBC F580-02	08-02-2015	5	20	20	2000
UGC3968	08-02-2015	10	10	20	2000
1300+0144	21-05-2015	5	20	20	2000
PGC60365	12-10-2014	5	6	20	600
CGCG 006-023	09-12-2014	5	10	20	1000
1252+0230	31-12-2014	5	15	20	1500
LSBC F570-01	31-01-2015	5	10	20	1000
1442+0137	21-05-2015	5	20	20	2000
LSBC F675-01	21-05-2015	5	15	20	1500
IC 2423	21-05-2015	5	10	20	1000

**Table 3.** The optical observations of galaxies UGC 11754 and UM 163.

Galaxy	date	Total exposure time (s)
UM 163	2014-07-07	300
UGC 11754	2014-07-07	300*3

ual frames, so that the bad frames can be avoided. All the good NIR frames were selected and preprocessing steps were done which included bias subtraction and flat fielding. The flat fielded frames, which were taken in different dither positions were aligned and combined. For the astrometry, we have found the centres of the sources in the field of view of the target frames using IMEXAM task in IRAF<sup>1</sup> and compared those with the 2MASS images, which were retrieved from the data archive. We used the python program for incorporating the world coordinate system (WCS) coordinate information in the images. The J, H and  $K_s$  images of each of the galaxies are shown in Figure 1. The J and H images of LSBC F584-01, the H images are UGC 3968 and 1300+0144 were not good since the sky conditions were bad due to the passing clouds. The  $K_s$  band isophotes are overlaid on the  $K_s$  band images. The J- $K_s$  images were created by dividing the J band images with  $K_s$  band images using task IMARITH, after the preprocessing steps such as dark subtraction, flat fielding, aligning and combining. The point spread function for J and  $K_s$  bands are similar, so that we directly divided the images with out any smoothing. The J- $K_s$  images are shown in figure 2.

The optical images of galaxies UM 163 and UGC 11754 were reduced using standard tasks in IRAF. The target frames were bias subtracted and flat field corrected. Cosmic ray hits were removed using the task COSMICRAYS. The frames were aligned together using GEOMAP & GEOTRAN tasks and combined using IMCOMBINE. The optical images are shown in figure 3.

## 5 IMAGE ANALYSIS

The reduced image frames were analysed using the tasks in the package STSDAS<sup>2</sup>. In the following section we describe how we fitted the ellipses and derived the deprojected bar lengths.

### 5.1 Individual galaxy notes on J, H images & $K_s$ band isophotes

The bar is clearly visible in the NIR images and represents the red, old stellar population of the disk. The  $K_s$  band isophotes trace the stellar density. In most of the cases the LSB galaxy disks are found to host big, bright bulges; these have been discussed in earlier studies of bulges in LSB galaxies (Galaz et al. 2002). The diffuse stellar disk are barely visible in NIR for most of the sample. This can be due to two reasons : (i) they have a predominantly younger population of stars in the disk which can not be traced very well

in the NIR bands. However, most LSB disks show very little star formation. (ii) Instead, it is more likely that the surface mass density of the stellar disks ( $\Sigma_*$ ) are very low and hence show very little structure in either NIR or optical images.

Isophotal contours in  $K_s$  do not show any significant twisting in the bar region for the sample galaxies. This suggests that the stellar orbits are aligned along the bar major axes ( $x_1$  orbits) (Das, Anantharamaiah & Yun 2001; Sormani, Binney & Magorrian 2015). If there are stellar orbits perpendicular to the bar length ( $x_2$  orbits), they will be apparent in the  $K_s$  contours, but most of our sample show simple, nested, contours aligned along the bar major axis. Just from visual inspection about half the sample of 29 galaxies in Figure 1 have bright, classical bulges. The remaining have either boxy bulges or are bulgeless. Several galaxies have short oval bars and boxy bulges as well. These systems may represent bars that are undergoing secular evolution and may finally evolve into large, boxy bulges. (Kormendy & Kennicutt 2004). The galaxies are individually described below.

CGCG 381-048- It has a long thin bar which is clearly visible in all J, H and  $K_s$  bands. Bulge is small but brighter. Disk is very diffuse and hardly visible for short exposures.

UGC 1920- has a oval bar with a bright, classical bulge. Disk features are very faint.

UGC 1455- The galaxy has a roundish, diskly bar. Classical bulge. Very bright and covers a large fraction of the bar. The disk is faint.

NGC 5905- Long thin bar and a bright, classical bulge. Traces of spiral arms and a corotation ring are visible in the NIR images.

UM 163- Long thin bar and a large, classical bulge. But the disk is very faint.

UGC 11754- Has an oval shaped, short bar. No clear bulge. Disk features are visible.

PGC 68495- Disky, oval bar. Small bulge. Galactic disk is diffuse and faint.

UGC 2936- Highly inclined galaxy that has a short, oval bar and distinct spiral arms. The disk spiral arms are surprisingly clear.

UGC 10405- Very short bar with a bright bulge. Disk is poorly seen.

0223-0033- Bright bulge with a small, oval bar followed by the spiral arms. The galactic disk is clearly visible in all the three bands.

UGC 5035- Small, oval bar and a large, classical bulge.

UGC 9087- Long bar with bright classical bulge. Disk is very faint.

LSBC F568-08- Short, oval bar. No clear bulge. Maybe a bar evolving into a bulge.

LSBC F568-09- Short bar with bright, classical bulge. The bar isophotes are diskly.

UGC 9634- Oval bar and a bright boxy bulge. Maybe undergoing secular evolution.

<sup>1</sup> Image Reduction & Analysis Facility Software

<sup>2</sup> The Space Telescope Science Data Analysis System (STSDAS) is a software package, which is used for reducing and analyzing astronomical data.



IC 742- Faint but long bar with bright, oval bulge. Stellar disk is slightly seen.

UGC 8794- Boxy bulge and short bar.

UGC 9927- Thick bar associated with a bright, classical bulge. Inner ring withing the bulge is visible.

LSBC F584-01- The weather conditions during the observation were not good which is reflected in the images. The galaxy has a short, oval bar.

LSBC F580-02-This galaxy does not have a proper bulge. The isophotes show a thin bar formed in the diffuse stellar disk.

UGC 3968- The observations in the H band were interrupted by the clouds. The galaxy has a long thin bar and a bright oval bulge.

1300+0144- The sky conditions were bad during the H band observations. The galaxy is has a short bar but no bulge.

PGC60365- Bright, oval bulge and only a faint bar. May represent ongoing secular evolution.

CGCG 006-023- Classified as not barred in NED. But has a bright, classical bulge and a clear bar.

1252+0230- Short, oval bar which associated with a bright, oval bulge. May represent ongoing secular evolution.

LSBC F570-01 - Very large oval bulge or bar.

IC 2423 - Short bar and compact bulge.

1442+0137 - Small bar and small, compact bulge.

LSBC F675-01-Small bar with oval bulge. May represent ongoing secular evolution.

## 5.2 Ellipse fit for NIR images

We used the IRAF task ELLIPSE to find the bar length and ellipticities using the  $K_S$  band images of the galaxies. The galaxy centers were first estimated using the task IMEXAM; the output obtained was given as the input for the task IMCNTR to determine the galaxy center more accurately. These values for the galaxy centers were taken as the input for the task ELLIPSE. An initial guess for the position angle was also made from visual inspection. During the fitting procedure, nearby sources were masked in order to avoid a bias in fitting procedure. We compared the outputs with and with out fixing the center of the galaxy. We first did the fitting without fixing the center and analyzed the output tables with the plotting task ISOPALL. For galaxies that had good signal to noise, such as UGC 3968, UGC 9927, IC 2423, even without fixing the center gave good fitting results. We further checked its stop code values to ensure the quality of the fit. However, for galaxies with poorer signal, the coordinates of the center can change from the central regions to the outer parts by more than two pixels. For these galaxies we redid the fit by fixing the center to the values obtained from the well fitted inner regions; we followed this method for the galaxies IC 742, UGC 8794, CGCG 006-023.

The bar semi major axis length and ellipticities were assumed to be the radii at which the surface brightness, ellipticity, position angle and b4 parameters changed abruptly. An example is shown in Figure 4. In the surface brightness plots, the initial sudden drop in the surface brightness near the center represents the bugle regions. After that it remains flat, this represents the contribution from the bar. At further radii the decrease in surface brightness represents the disk region. In the ellipticity plots (where ellipticity is de-

fined as  $1-b/a$ , where  $b$  and  $a$  are the semi-minor and semi-major axes respectively) (Jedrzejewski 1987), except for a few pixels in the centre, the ellipticity initially increases, reaching a maximum value and remains at a constant value for a few pixels. Then the ellipticity decreases suddenly, this corresponds to the bar end. Similarly the position angle plot also has distinct regions for the different galaxy components. The b4 parameter reveals the diskyness or the boxyness of the fitted ellipse and by how much the fitted ellipse differ from the actual isophotes. For example the b4 parameter of UGC 3968 indicates the bar has a boxy shape.

The increase in semi major axis at each level is 0.1 times the semi major axis of the previous level. All the parameters obtained through the fitting procedure with their error measurements are tabulated in Table 3.

## 5.3 Deprojecting the bar length

The observed image is the projected image of the galaxy on the sky. So the bar length and ellipticities that we observe are not the intrinsic parameters of the bar. We deprojected the bar length and ellipticity using the following derived parameters - position angle of the galaxy, angle of inclination of the galaxy and the parameters obtained from ellipse fit such as the bar semi major axis length, position angle of the bar with respect to the major axis of the galaxy and the bar ellipticity. The inclination and the position angle of the galaxies were taken from NASA Extragalactic Database (mainly from the RC3 catalogue and SDSS). Since the two surveys cover two different wavelength bands, the redder indicating the older population and the bluer band tracing the young stellar population, their values are connected with the intrinsic properties of the galaxy and give a good estimate of the size of the stellar disks. We selected the values corresponding to the 25 mag/arcsec<sup>2</sup> isophote. However, for the galaxies which are covered in both the surveys, we selected the higher 25 mag/arcsec<sup>2</sup> sizes to obtain an upper estimate of the galaxy diameter. The angle of inclination can be found from the  $\cos^{-1}(b/a)$  values, where  $b$  is the semi minor axis and  $a$  is the semi major axis of the galaxy as derived from the isophotes.

For galaxies LSBC F580-02 and PGC 60365 the parameters were not listed in the literature, so we have taken their SDSS r-band images and fitted ellipses using the task ELLIPSE in IRAF. The position angle of the galaxy and the angle of inclination were determined from the fitted 25 mag/arcsec<sup>2</sup> isophote. For the galaxy UGC 11754 there was no literature value and no SDSS image; also for UM 163 the position angle is not in the literature and the SDSS image was on the edge of the frame so half of the galaxy image was cut out of the frame. Hence we have taken a r-band images of these galaxies, UGC 11754 and UM 163 using the HCT. We have the J, H,  $K_S$  band images of both galaxies but the galaxy disk is poorly visible. We did the ELLIPSE fit, determined the position angle and the  $(b/a)$  value of the outer most isophote from the r-band images.

If the galaxy is inclined at an angle  $i$ ,  $\alpha$  is the angle between the bar major axis and the galaxy axis in the sky plane and  $L_{obs}$  is the observed bar semi major axis length in the sky plane, then the intrinsic barlength can be determined from the following relation (Gadotti et al. 2007;

Martin 1995)

$$L_{dep} = L_{obs} (\sin^2 \alpha \sec^2 i + \cos^2 \alpha)^{1/2}$$

The  $L_{dep}$  can be converted to the physical units  $L_{bar}$  which is in kpc using the scale for the galaxy. However, this relation is derived using a 1-D approximation, in which the bar is considered as a line. In actual case, the bar is not a 1-D line but has a 2-D shape. However, the relations will work well for  $i$  less than  $60^\circ$ . The uncertainties in deprojection will increase with increasing  $i$  and all the deprojection methods behave badly when the inclination angle  $i$  is larger than  $60^\circ$  (Gadotti et al. 2007; Zou, Shen & Li 2014). Unfortunately some of our galaxies 0223-0033, UGC 2936, UGC 9634, UGC 8794 and 1300+0144 have high inclination angles; hence, the results for these galaxies will have greater error. So even though we calculated the bar parameters for these galaxies, we exclude them in the plots (Figures 5, 6, 7, 8). The deprojected parameters are tabulated in Table 4 with their errors obtained using the propagation of errors in the observed parameters.

#### 5.4 Deprojecting the bar ellipticities

Just like barlength, the observed ellipticities of the bars will also be different from the intrinsic values due to the projection effects. The deprojected ellipticity can be calculated analytically from the following observed parameters - bar major axis length, ellipticity, angle between the galaxy major axis and the bar major axis, the angle of inclination of the galaxy (Gadotti et al. 2007). In this method we consider the galaxy nodal axis to lie along the x-axis or abscissae. The bar is an ellipse in the rotated co-ordinate system in which the bar major axis is the x-axis of the rotated system. The entire galactic co-ordinate plane is inclined at an angle  $i$  with the sky plane. Using the general conic section equations for this system, we will get a quadratic equation. Solving this will give the semi-major and semi-minor axes values which can be used to get the deprojected ellipticities of the bars.

## 6 RESULTS

### 6.1 Distribution of barlengths and ellipticity of our sample

The histogram of the deprojected bar length, deprojected ellipticities and the ratio of barlength to  $D_{25}$  are shown in Figure 5. Most of the galaxies have bar lengths of 8 to 17 kpc which is similar to the NIR barlengths seen in normal galaxies. For normal galaxies the large scale bar sizes are in the range 2-28 kpc with 50 % of them clustered in the range of 4-10 kpc (Marinova & Jogee 2007; Menéndez-Delmestre et al. 2007). Thus surprisingly our plot does not show any special trends for bars in LSB galaxies. Some LSB galaxies such as UM 163, UGC 5035, UGC 8794, PGC 60365 have very large bar lengths greater than 18 kpc. The distribution of the ratio of barlength with the  $D_{25}$  diameter ( $D_{bar}/D_{25}$ ) peaks in the 0.4 to 0.6 range, which is also in good agreement with the bars observed in normal barred galaxies, for which this fraction is in the range of 0.1 to 0.5. It has been observed that bars in early type galaxies have  $D_{bar}/D_{25}$  twice as large compared to late type spirals (Menéndez-Delmestre et al. 2007). However, although LSB galaxies are extreme late type

spiral galaxies, we find that their bar lengths  $D_{bar}/D_{25}$  are not confined to low values as expected for late type spirals.

These results are surprising since early studies have shown that bars are difficult to form in dark matter dominated galaxies (Ostriker & Peebles 1973; Hohl 1976; Efsthathiou, Lake & Negroponte 1982). The low stellar mass surface density may also be a reason for the lower bar fraction in LSB galaxies (Mihos, McGaugh & de Blok 1997). Since the barlength is a measure of the global instability formed in a disk and the instability length scale, we would also expect bars in halo dominated galaxies such as LSB galaxies to be shorter. The presence of a range of barlengths suggests that it is not just the halo mass that influences bar formation, but also perhaps the halo shape and spin plays an important role in bar formation in spiral galaxies (Athanasoula, Machado & Rodionov 2013; Saha & Naab 2013a; Long, Shlosman & Heller 2014; Hoffman et al. 2007; Heller, Shlosman & Athanassoula 2007; El-Zant & Shlosman 2002; Martinez-Valpuesta & Shlosman 2004). Our study thus provides a test sample in which to study the effect of halo parameters on bar formation in disk galaxies.

The ellipticities also show a similar trend. The histogram peaks in the ellipticity range 0.4 to 0.6 (Figure 5). There are very few cases that exhibit low ellipticity values (say the range of 0.2 to 0.3); some galaxies show very high values of ellipticity which is not expected for bars in late type, dark matter dominated galaxies. For normal barred galaxies the ellipticity lies in the range 0.5 to 0.75 (Marinova & Jogee 2007; Menéndez-Delmestre et al. 2007). All these suggest that the bars in LSB galaxies are similar to the bars in normal galaxies. In figure 6, we have plotted the ellipticity against the ratio of barlength to  $D_{25}$  ( $D_{bar}/D_{25}$ ). The LSB galaxies here also show a scattered distribution similar to normal galaxies.

### 6.2 Variation of bar properties with the gas fraction

We have investigated the variation of bar properties with the baryonic masses of the galaxies. Since molecular gas is usually low or absent in LSB galaxies (Das et al. 2006) we assume the baryonic mass to be the sum of the stellar mass and neutral hydrogen mass in LSB galaxies. For stellar mass calculation we have used the model magnitudes and fluxes from the SDSS DR12 database. The SDSS (g-r) colors were converted into corresponding (B-V) values using the color relation  $B-V = 0.98 \times (g-r) + 0.22$  (Jester et al. 2005). Using the (B-V) color and the R-band flux values we have calculated the mass of the underlying stellar population using the color dependent mass to light ratio coefficient. Given for the closed box model (Bell & de Jong 2001). The (g-r) & (B-V) colors and stellar masses are listed in the Table 5.

We have taken the H1 fluxes from HYPERLEDA database and calculated the neutral hydrogen masses ( $M(HI)$ ) using the relation  $M_{HI} = 2.36 \times 10^5 D^2 \int (Sd\nu) M_\odot$  (Roberts 1975), where  $D$  is the distance to the galaxy in Mpc and flux integral is in  $Jy \text{ Km s}^{-1}$ . The H1 mass for each of the galaxies are listed in Table 6. Since the LSB galaxies are poor in molecular hydrogen and dust, the total baryonic mass is calculated as the sum of stellar mass and the H1 mass. Figure 7 (top) shows the plot of the relative bar length  $D_{bar}/D_{25}$  against  $M(HI)$  normalized by the total baryonic

mass (i.e.  $M_{HI}/M_{HI}+M_{stellar}$ ). Figure 7 (middle) shows the bar ellipticity plotted against the  $M_{HI}/M_{HI}+M_{stellar}$ . Neither shows any correlation and there is a lot of scatter. The lower plot shows the variation of bar length  $D_{bar}/D_{25}$  with the total baryonic mass. There is only a weak correlation. Simulations have shown that gas fraction can severely limit the secular bar growth (Villa-Vargas, Shlosman & Heller 2010). However, we do not see any variation of bar properties with HI masses in our sample of LSB galaxies, even though the HI gas fraction of the baryonic mass is as large as 20 to 50%.

### 6.3 The J- $K_s$ color plots

Most of our J, H,  $K_s$  images do not have much emission from the stellar disks, possibly because of the low stellar surface density (Figure 2). The exceptions are CGCG 381-048, NGC 5905 and UGC 3968, which show faint emission from their disk regions. Hence, most of our (J- $K_s$ ) color images (i.e. the J and  $K_s$  flux ratios) mainly reveal the difference in stellar emission from the bulge and bar regions only. The (J- $K_s$ ) images in general show only a very narrow brightness range or color gradient, indicating that the stellar population and metallicity in the bar and bulge regions are very similar; or in other words the color profile is flat. It also shows there is not much dust content in these LSB galaxies which is expected from earlier Spitzer observations of LSB galaxies (Rahman et al. 2007; Hinz et al. 2007). Although the gradient over the bar is very small in the color plots, in some galaxies the bulge is dark with respect to the bar. This indicates that the J and  $K_s$  flux ratios are very low in those bulges which shows that are composed of an older stellar population than that of the bar. Below we briefly summarise the J- $K_s$  plots (Figure 2).

(i) For the galaxies CGCG 381-048, UGC 11754, PGC 68495, UGC 10405, UGC 5035, 0223-0033, UGC 9087, UGC 3968, 1300+0144, PGC 60365, CGCG 006-023, 1252+0230 the (J- $K_s$ ) color of their bulge and bar regions are almost the same i.e. they have a flat color gradient. We can conclude that the bulge and bar have almost similar stellar populations and low dust content.

(ii) The galaxies UGC 1920, UGC 1455, NGC 5905, UM 163, UGC 2936, LSBC F568-08, UGC 9634, IC 742, UGC 8794, UGC 9927, LSBC F584-01, LSBC F580-02 show significant variations in color for the bar and central bulge regions, indicating the central bulge is made up of older stellar population.

(iii) In some galaxies like CGCG 381-048, NGC 5905, UGC 11754, 0223-0033, UGC 3968, PGC 60365, CGCG 006-023 the disk and the bar show similar colors in their bars and bulges. In these galaxies bar might have helped the mixing of stellar population and metallicity.

(iv) In case of the galaxy UGC 2936, even the spiral arms are visible in the disk representing the arm of older stars. this galaxy may have significant dust and ongoing star formation (Pickering et al. 1999).

### 6.4 Variation of J- $K_s$ with bar parameters

We were not able to get the NIR standard star observations on the same day as our observation for most of our sample. Alternatively, we could have used NIR bright stars in

our observing frames. But unfortunately most of our NIR frames did not have a good enough number of stars that did not show NIR variability for calibrating the NIR magnitudes. Hence to have uniform magnitudes we have used the J, and  $K_s$  magnitudes from the 2MASS catalogue for extended sources for most of our sample galaxies (Table 6) (Skrutskie et al. 2006); for some it was not available. The J and  $K_s$  magnitudes with their errors are listed in table 6. To see if whether the bar parameters are directly show any correlation with the color of the galaxy, we have plotted the J- $K_s$  values with the bar deprojected ellipticities and the ratio of barlength to the disk size  $D_{bar}/D_{25}$ . The plots are shown in Figure 8. The bar ellipticities show a weak relation with the J- $K_s$  color. But the relative bar lengths  $D_{bar}/D_{25}$  show a clear correlation with the J- $K_s$  colors. This is because a longer bar that extends further into the disk will trigger more star formation and thus make the galaxies bluer.

### 6.5 J- $K_s$ variation with stellar and neutral hydrogen masses

Figure 9 shows the J- $K_s$  color plotted against the ratio of neutral hydrogen mass to stellar mass ( $M_{HI}/M_{stellar}$ ). The J- $K_s$  color of the galaxies do not exhibit any strong correlation with the ratio  $M_{HI}/M_{stellar}$ . For normal galaxies those hosts strong bars, the bars can trigger disk star formation and gas infall (Ellison et al. 2011; Renaud et al. 2015). Hence, bluer colors maybe correlated with more gas depletion or lower gas mass fractions  $M_{HI}/M_{stellar}$ . If that is true for our sample of LSB galaxies, Figure 9 should show decreasing J- $K_s$  values with increasing  $M_{HI}/M_{stellar}$  ratios. However, we do not see any correlation at all, which suggests that the bars in LSB galaxies are not strong enough to trigger enough star formation to cause significant gas depletion in their disks. However, star formation maybe episodic in nature (Mishra et al. 2015) and localized to small regions in the disk.

## 7 COMPARING OUR OBSERVATIONS WITH SIMULATIONS IN THE LITERATURE

Early simulations have shown that cold rotating stellar disk will become bar unstable (Ostriker & Peebles 1973). Later simulations showed that if the stellar disks are immersed in massive dark matter halos, the disc will be stable against bar formation. In these studies the halos were both non-rotating and non responsive i.e they were fixed potentials (Hohl 1976; Efstathiou, Lake & Negroponte 1982). Later simulations of halo dominated LSB galaxies have shown that they are usually stable against bar formation but if bars do form, they are smaller than those found in normal galaxies (Mihos, McGaugh & de Blok 1997; Mayer & Wadsley 2004). The lower fraction of barred LSB galaxies obtained in our sample selection (Section 2) supports these early simulations.

However, our observations clearly show that halo dominated galaxies can host strong bars (e.g. NGC 5905, IC 742, UGC 8794). This is where our observations differ from early simulations and it is the most important result from our study. Our observations suggest that it is not just the relative disk to halo mass that determines whether a bar can

form in a disk galaxy, other parameters such as the halo angular momentum and halo shape can influence bar formation and determine the bar strength and shape. Some simulations with live or responsive halos have shown that the halo concentration can have a pronounced effect on the bar formation (Villa-Vargas, Shlosman & Heller 2009) and not the total mass of the halo. In the simulations, the spinning dark matter halos helps in the bar formation (Saha & Naab 2013b; Long, Shlosman & Heller 2014). Besides these factors the axes ratios or the shape also can influence the bar growth considerably even for massive halos (Athanasoula, Machado & Rodionov 2013). In these studies, the halo is composed of N-body particles just like the disk; there is angular momentum transfer between the stellar disk and halo (Weinberg 1985; Debattista & Sellwood 1998; Villa-Vargas, Shlosman & Heller 2009) which helps the disks form strong bars despite the large halo masses. In short the responsive halos can form strong bars (Athanasoula 2002; Athanasoula 2003). The bar-halo interaction can also result in the slow down of bar rotation in later evolutionary stages (Chemin & Hernandez 2009). In the secular phase the bar growth triggered by buckling instabilities and vertical resonances will alter the bar shape, and transform the bar into peanut or boxy shapes (Martinez-Valpuesta, Shlosman & Heller 2006; Combes et al. 1990). LSB galaxies also show signatures of secular evolution since several galaxies in our sample appear to have boxy bulges (e.g. 1252+0230, PGC 60365, UGC 8794) (Sheth et al. 2005). We are exploring this in a separate study. Thus LSB galaxies are an important testbed for understanding the evolution of galaxy disks in halo dominated environments.

## 8 CONCLUSIONS

1. The fraction of bars in LSB galaxies is very low, as expected from the simulations of bar formation in halo dominated galaxies. We examined the SDSS images of a sample of 856 LSB galaxies and found that only 8.3% have bars. This low fraction supports the simulations that show that massive dark matter halos suppress the formation of disk instabilities such as bars in spiral galaxies.
2. About half our sample of 29 barred LSB galaxies host large, classical bulges that are very bright in the NIR. The remaining other half have either boxy bulges or are bulgeless. The bars are also much brighter in NIR than the diffuse stellar disks. This indicates that both the bars and bulges have either an older stellar population and/or higher stellar surface density than the LSB disks. The  $K_s$  isophotes do not show any twisting in the selected sample and are instead generally aligned along the bar major axes.
3. Although the fraction of barred candidates in the dark matter dominated LSB galaxies is very small, the bar parameters such as bar length and ellipticities have a range of values that are similar to those found in normal galaxies. Our results clearly show that halo dominated galaxies can host strong bars.
4. For more than half of the sample (25/29) the color parameter  $J-K_s$  shows practically no variation between the bar and bulge regions. This indicates that they have similar stellar populations, metallicities and dust content. Some candidates have bulges that are significantly dimmer than the

bar; these galaxies may have a older cold stellar population in the bulge.

5. The plots of  $J-K_s$  with the bar length  $D_{bar}/D_{25}$  shows a weak but significant correlation, which suggests that the bar may cause some local disk star formation which makes the  $J-K_s$  bluer. But the plots of  $J-K_s$  with the ratios of the HI content and stellar mass ( $M_{HI}/M_{stellar}$ ) do not show any correlation, which clearly shows that the star formation triggered by the bar is only local and not on a global disk scales.

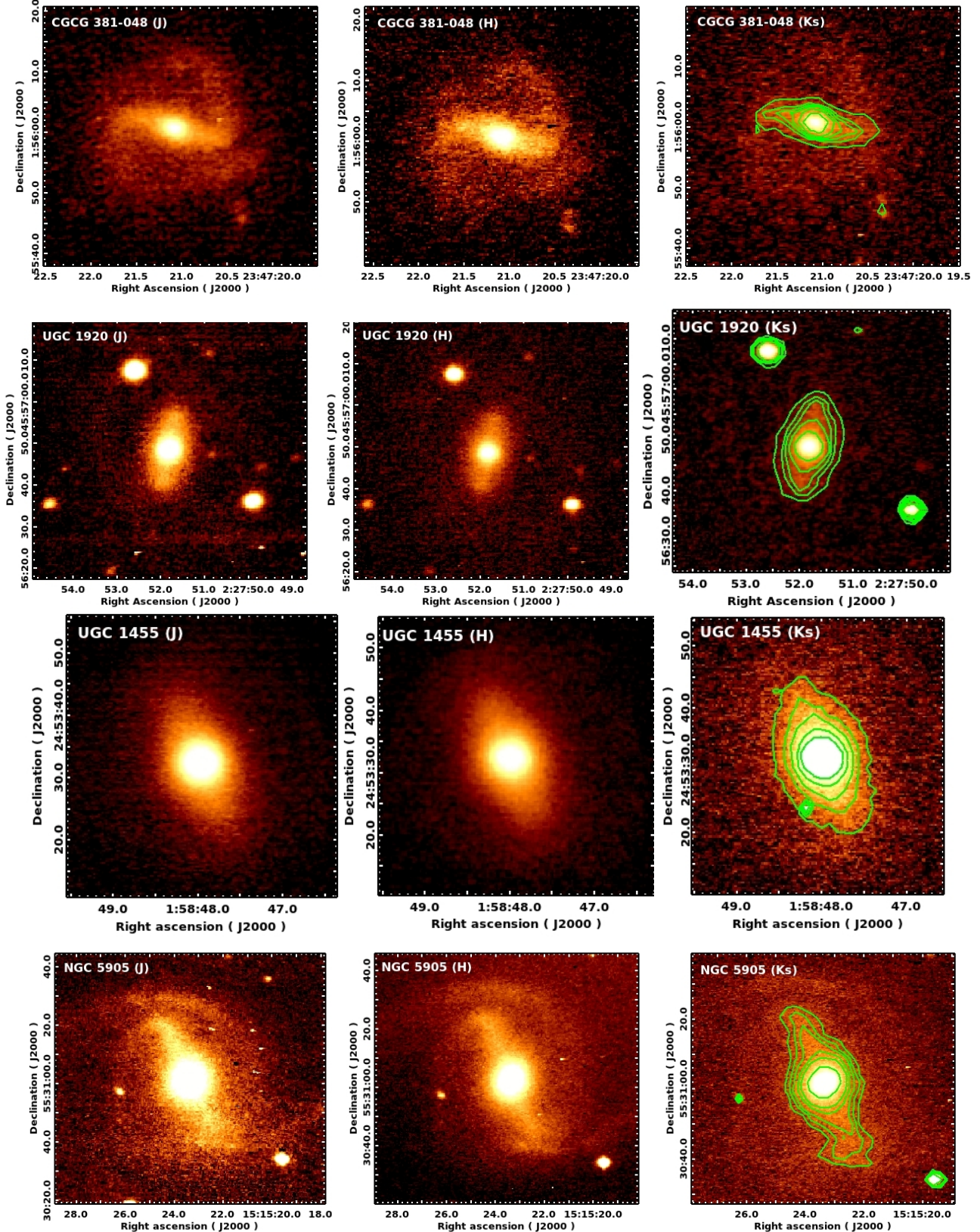
## ACKNOWLEDGMENTS

The optical observations were done at the Indian Optical Observatory (IAO) at Hanle. We thank the staff of IAO, Hanle and CREST, Hosakote, that made these observations possible. The facilities at IAO and CREST are operated by the Indian Institute of Astrophysics, Bangalore. This research has made use of the NASA/IPAC Extragalactic Database (NED), which is operated by the Jet Propulsion Laboratory, California Institute of Technology, under contract with the National Aeronautics and Space Administration. We acknowledge the usage of the HyperLeda database<sup>3</sup> (Makarov et al. 2014). Our work has also used SDSS-III data. Funding for SDSS-III has been provided by the Alfred P. Sloan Foundation, the Participating Institutions, the National Science Foundation, and the U.S. Department of Energy Office of Science. The SDSS-III website is <http://www.sdss3.org/>. SDSS-III is managed by the Astrophysical Research Consortium for the Participating Institutions of the SDSS-III Collaboration including the University of Arizona, the Brazilian Participation Group, Brookhaven National Laboratory, Carnegie Mellon University, University of Florida, the French Participation Group, the German Participation Group, Harvard University, the Instituto de Astrofisica de Canarias, the Michigan State/Notre Dame/JINA Participation Group, Johns Hopkins University, Lawrence Berkeley National Laboratory, Max Planck Institute for Astrophysics, Max Planck Institute for Extraterrestrial Physics, New Mexico State University, New York University, Ohio State University, Pennsylvania State University, University of Portsmouth, Princeton University, the Spanish Participation Group, University of Tokyo, University of Utah, Vanderbilt University, University of Virginia, University of Washington, and Yale University. This publication makes use of data products from the Two Micron All Sky Survey, which is a joint project of the University of Massachusetts and the Infrared Processing and Analysis Center/California Institute of Technology, funded by the National Aeronautics and Space Administration and the National Science Foundation. This research made use of Montage. It is funded by the National Science Foundation under Grant Number ACI-1440620, and was previously funded by the National Aeronautics and Space Administration's Earth Science Technology Office, Computation Technologies Project, under Cooperative Agreement Number NCC5-626 between NASA and the California Institute of Technology. The color plots were generated using the two-dimensional graphics environment Matplotlib (Hunter 2007). We thank the anonymous referee for valuable comments and suggestions on the draft.

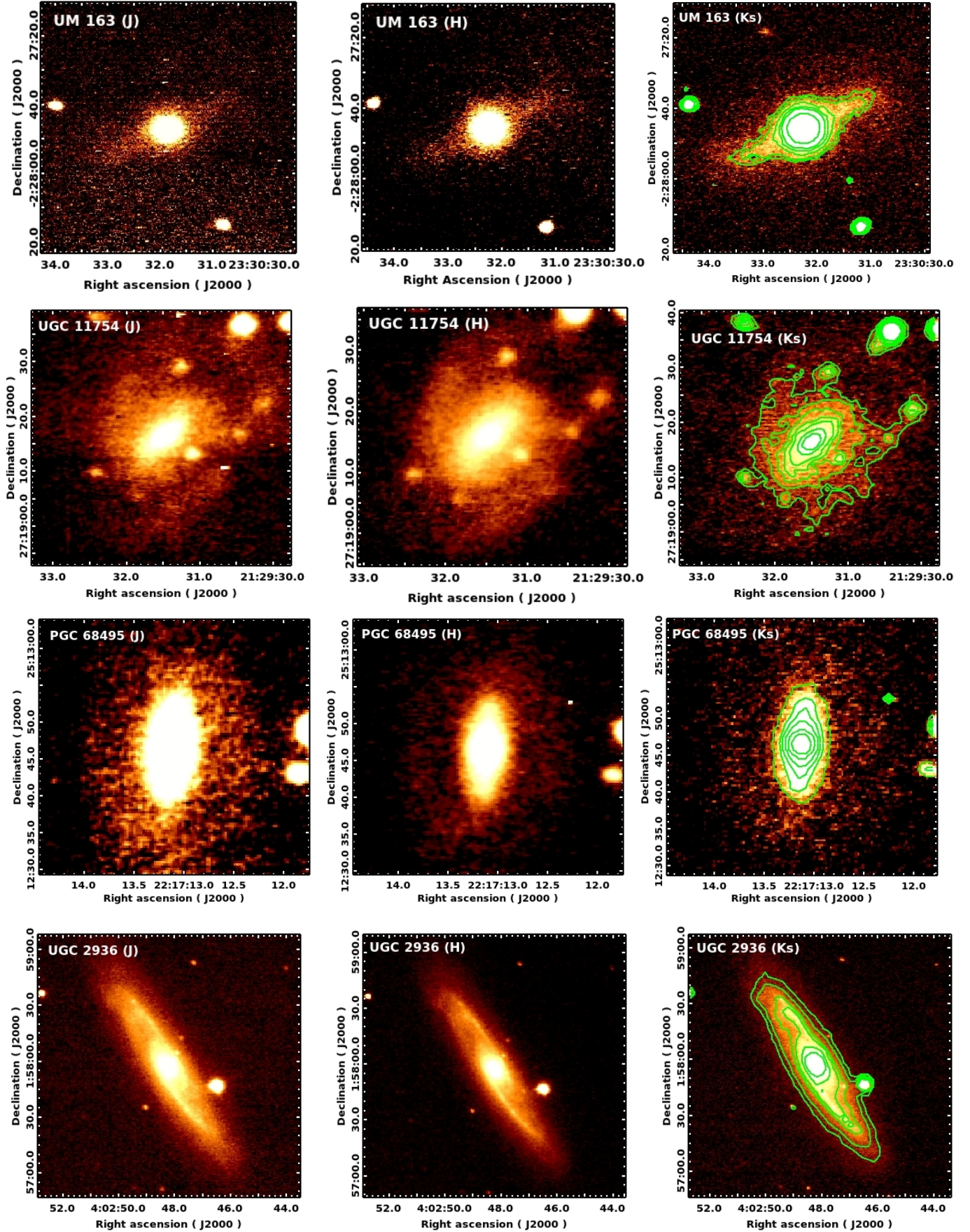
<sup>3</sup> <http://leda.univ-lyon1.fr/>



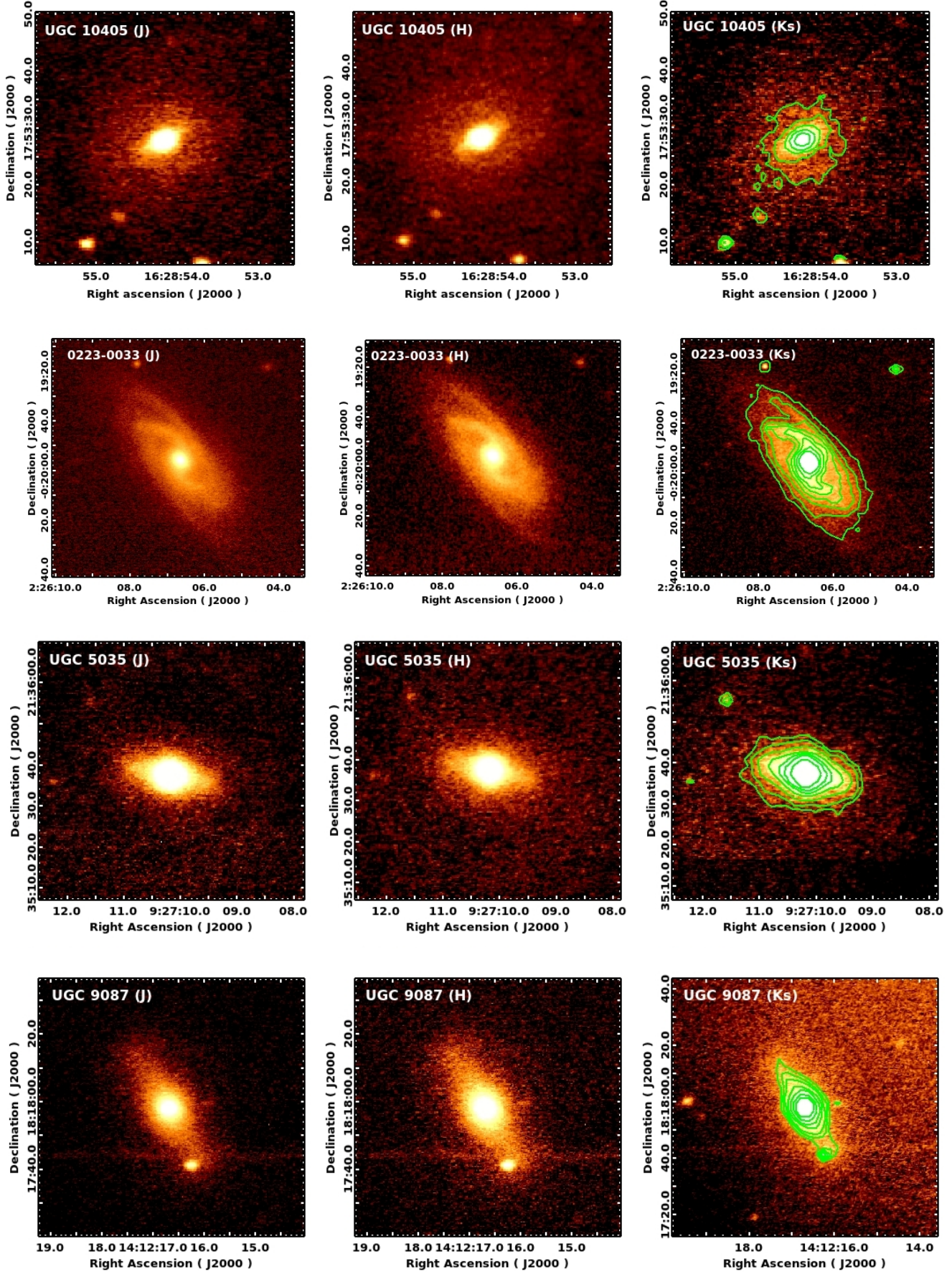
**Figure 1.** The J, H,  $K_s$  band images of Low Surface Brightness galaxies. In all figures the north is up and east is in the left hand side. We have used the logarithmic scaling. The isophotal contours are overlaid on the  $K_s$  band image. Most of the isophotes are above  $5\sigma$  level except the galaxies IC 742, NGC 5905, PGC 68495, UMI163, LSBC F568-08, UGC 5035, LSBC F568-09 have last contour level is  $4\sigma$  and for galaxies CGCG 381-048, UGC 1920, UGC 9927, UGC 9634 have last contour level is  $3\sigma$ . For galaxies UGC 3968, LSBC F580-01, and 1300+0144 the H band observations were effected by the bad sky conditions.



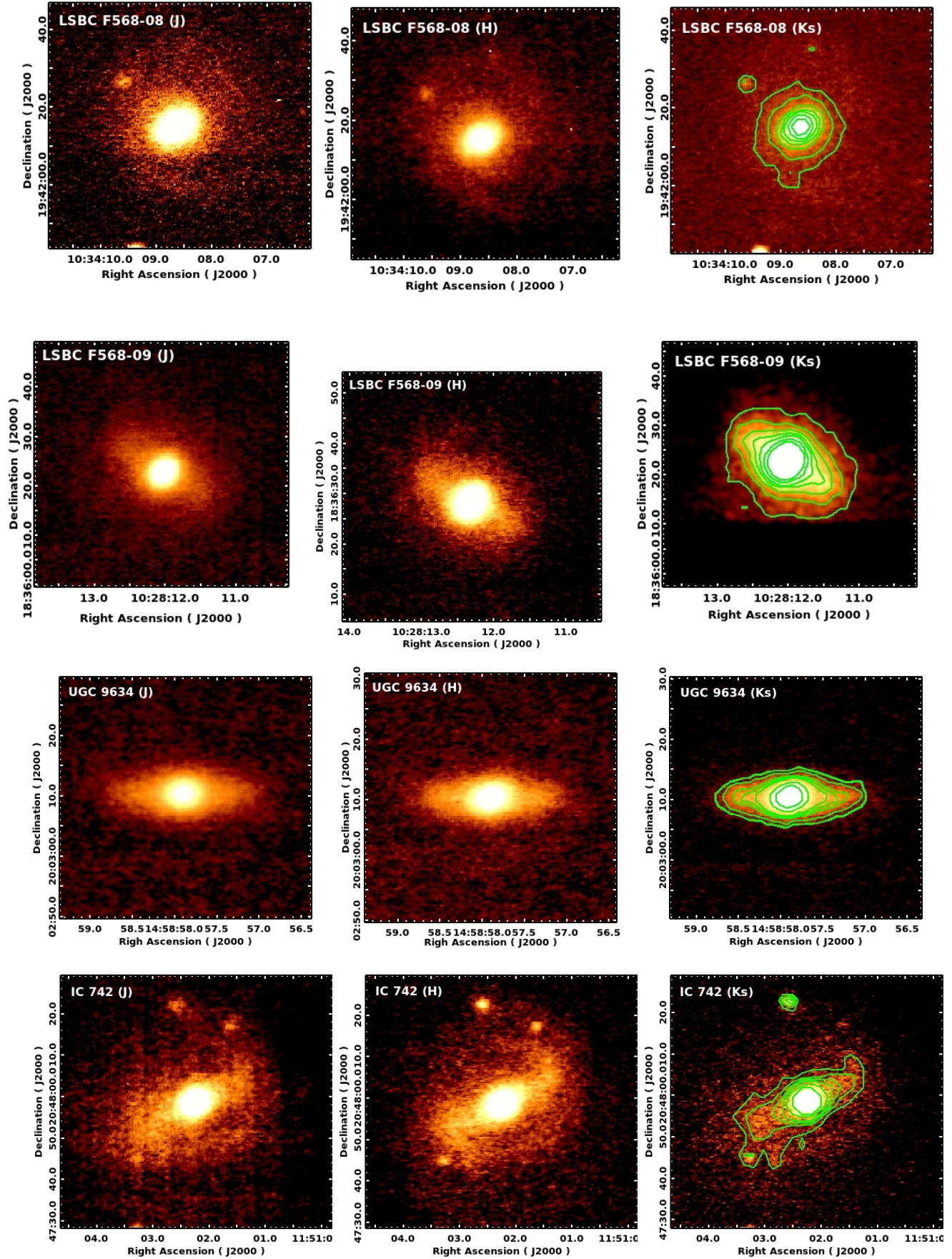




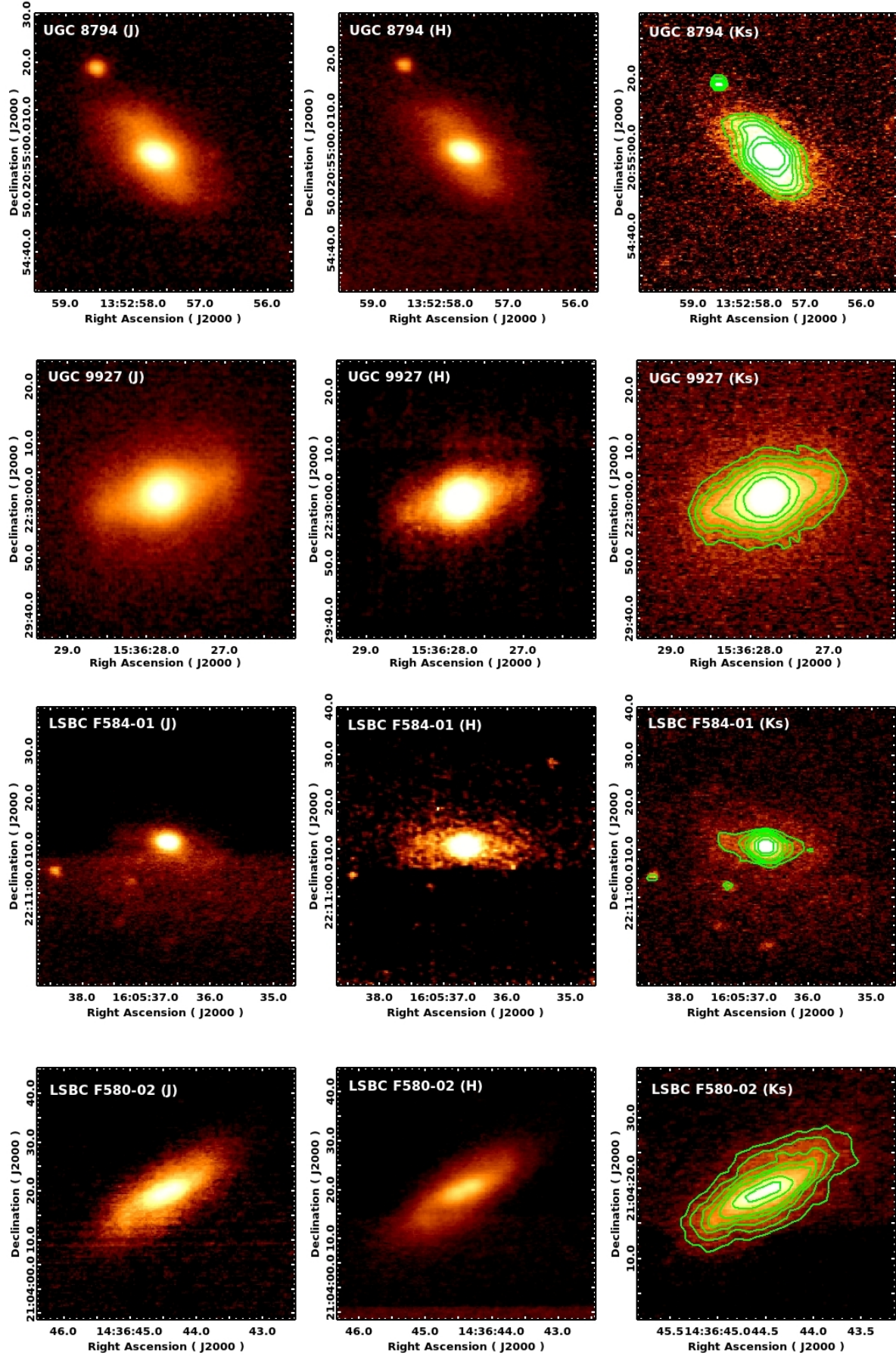


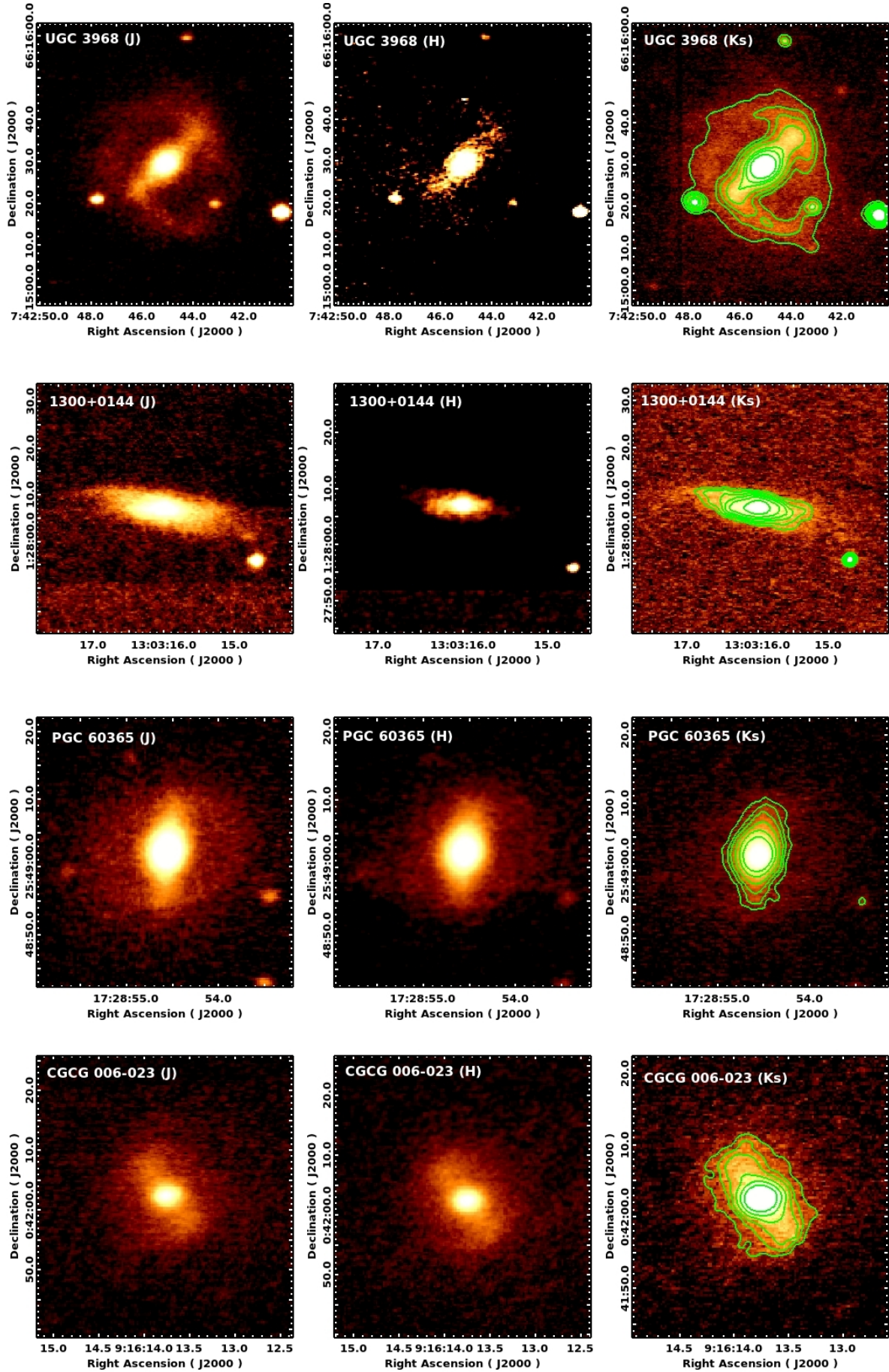




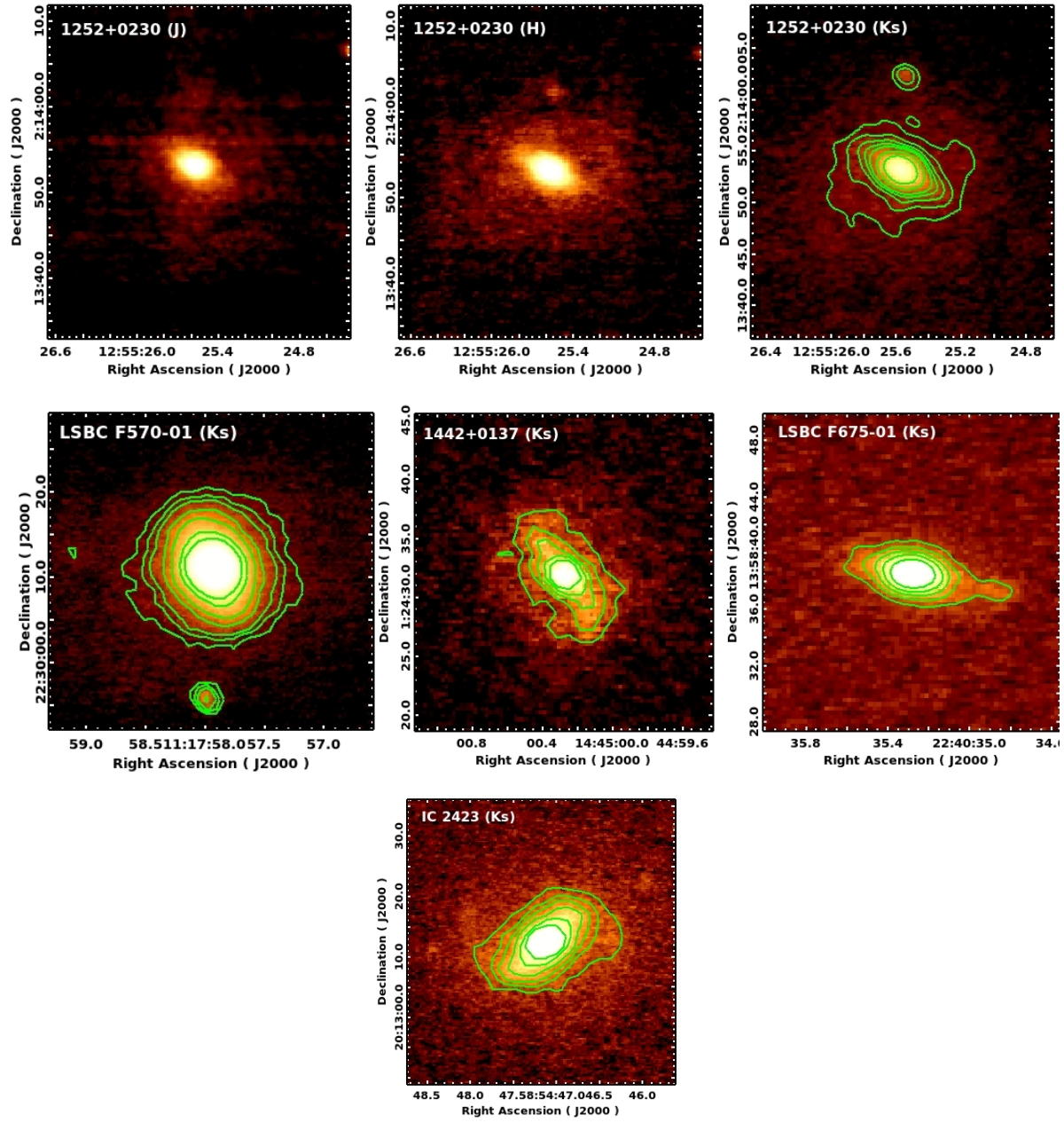




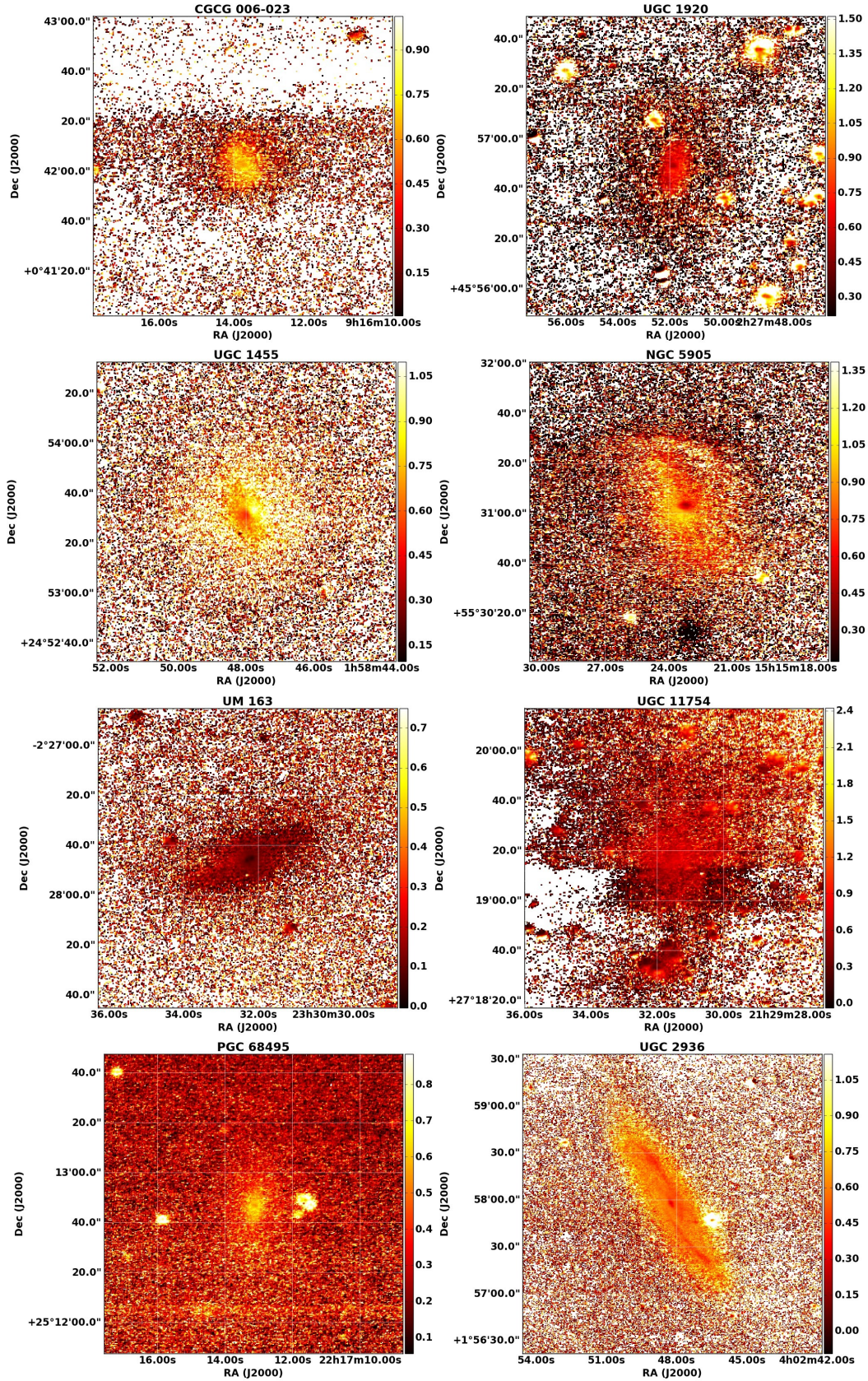




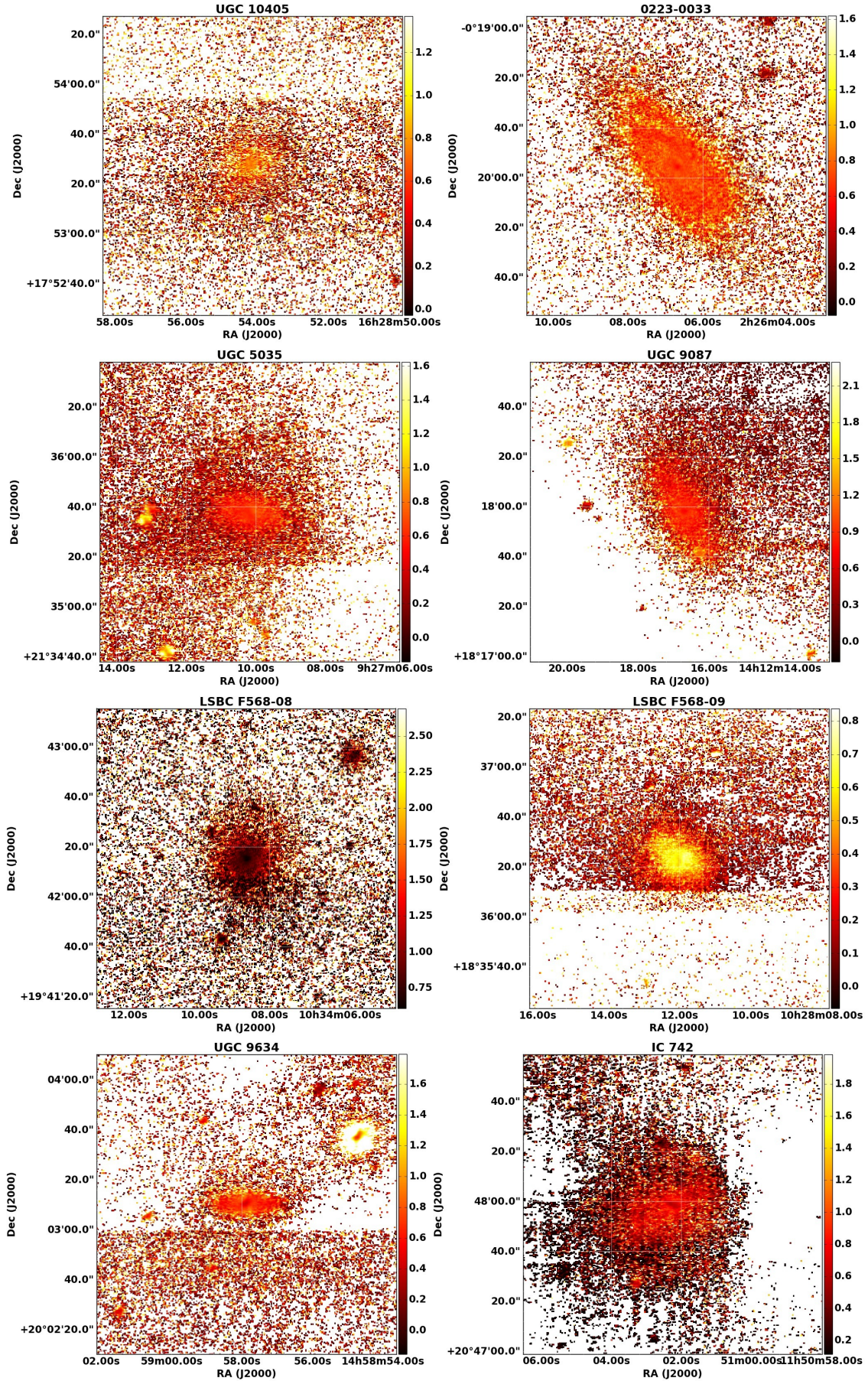




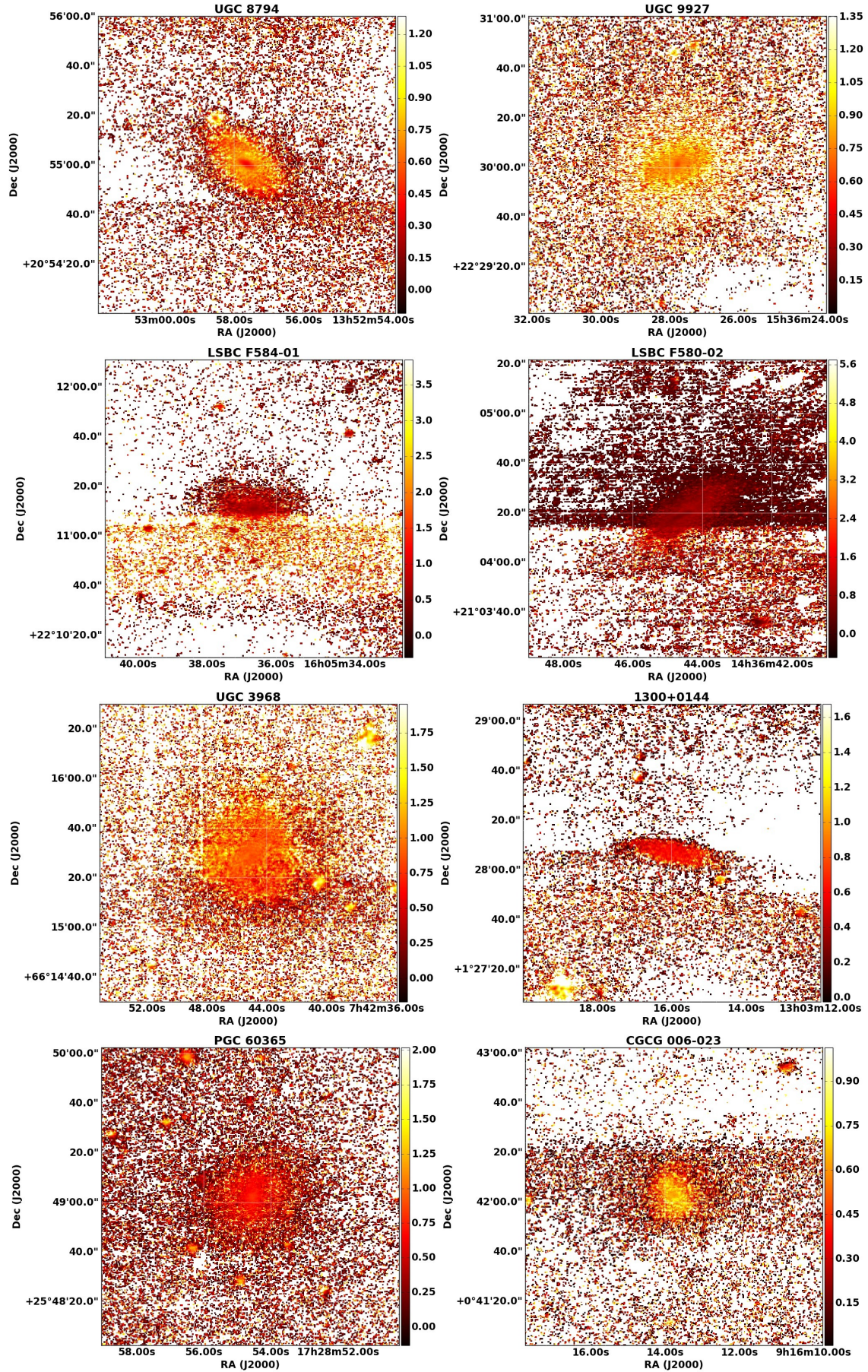


**Figure 2.** The J- $K_s$  images of Low Surface Brightness galaxies











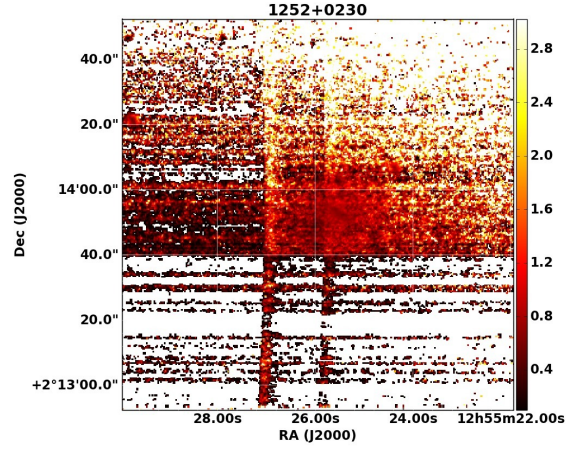
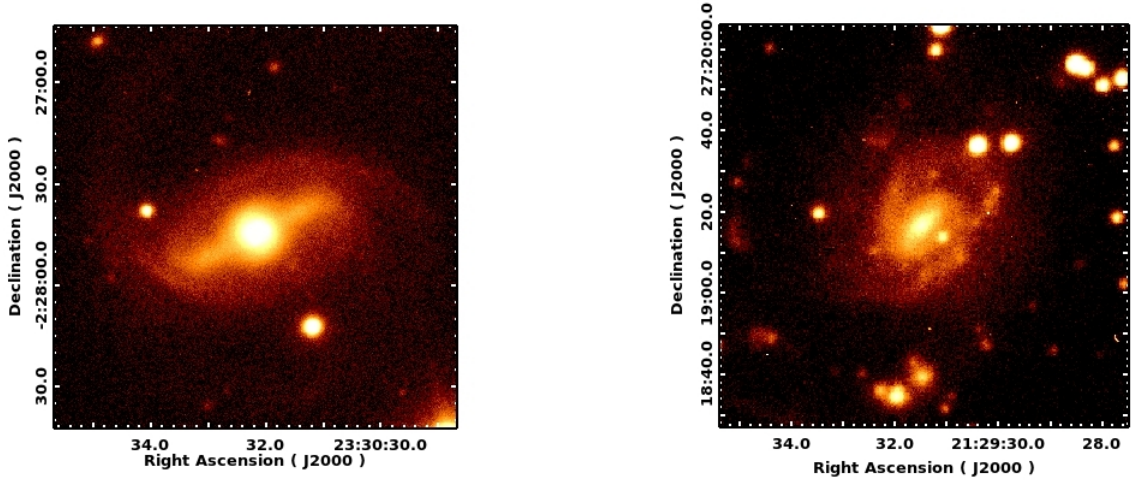


Figure 3. The R-band images of galaxies UM 163(left) and UGC 11754(right). Logscale is used in both of the images.



**Table 4.** The bar parameters of LSB galaxies from ellipse fit. The parameters  $a$  &  $b$  are the semi major and semi minor axis of the galaxy in RC3 or SDSS r-band depending upon which one is covering the galaxy disk at greater distance. The angle of inclination is given as  $i$ .  $L_{obs}$ ,  $e_{obs}$  and  $PA_{bar}$  is the projected bar semi major axis length, ellipticity and bar angle obtained from ELLIPSE fit.  $PA_{gal}$  is the position angle of the galaxy. The parameters  $b/a$ ,  $i$  and  $PA_{gal}$  are taken from NED. ( the position angles are taken from north to eastwards given in degrees). The difference between  $PA_{bar}$  and  $PA_{gal}$  is taken as  $\alpha$ .  $L_{dep}$  is the deprojected bar semi major axis length calculated in arcsec. The  $e_{dep}$  is the deprojected ellipticity. Using the scale given in table 1,  $L_{dep}$  is converted to physical units (kpc) given as  $L_{bar}$ . For galaxies 0223-0033, UGC 2936, UGC 9634, UGC 8794 and 1300+0144 are having high inclination angles that are greater than  $60^\circ$  so we are avoiding those galaxies for the plots even though listed in the table.

Galaxy name	$b/a$	$i$ ( $^\circ$ )	$L_{obs}$ (arcsec)	$e_{obs}$	$PA_{bar}$ ( $^\circ$ )	$PA_{gal}$ ( $^\circ$ )	$\alpha$ ( $^\circ$ )	$L_{dep}$ (arcsec)	$L_{bar}$ (kpc)	$e_{dep}$
CGCG381-048	0.78	38	$11.39 \pm 1.14$	$0.38 \pm 0.03$	$67 \pm 3.1$	42	25	$12.00 \pm 1.21$	$3.83 \pm 0.39$	$0.32 \pm 0.04$
UGC1920	0.72	44	$9.41 \pm 0.94$	$0.50 \pm 0.02$	$166 \pm 1.3$	10	24	$10.11 \pm 1.01$	$3.93 \pm 0.39$	$0.42 \pm 0.02$
UGC1455	1.00	0	$16.68 \pm 1.67$	$0.44 \pm 0.03$	$28 \pm 3.0$	132	76	$16.68 \pm 1.67$	$5.27 \pm 0.53$	$0.44 \pm 0.03$
NGC5905	0.66	49	$25.67 \pm 2.57$	$0.54 \pm 0.03$	$21 \pm 2.0$	135	66	$37.21 \pm 3.73$	$8.41 \pm 0.84$	$0.67 \pm 0.02$
UM163	0.69	46	$22.20 \pm 2.22$	$0.41 \pm 0.04$	$115 \pm 3.5$	99	16	$23.08 \pm 2.34$	$14.24 \pm 1.44$	$0.26 \pm 0.05$
UGC11754	0.89	27	$8.56 \pm 0.86$	$0.47 \pm 0.01$	$145 \pm 2.3$	157	12	$8.61 \pm 0.86$	$2.53 \pm 0.25$	$0.42 \pm 0.02$
PGC68495	0.65	50	$7.08 \pm 0.71$	$0.56 \pm 0.01$	$174 \pm 0.6$	117	57	$10.00 \pm 1.00$	$7.79 \pm 0.78$	$0.66 \pm 0.01$
UGC2936	0.27	74	$10.35 \pm 1.04$	$0.43 \pm 0.01$	$26 \pm 0.7$	30	4	$10.66 \pm 1.07$	$2.58 \pm 0.26$	$0.52 \pm 0.01$
UGC10405	0.74	42	$5.32 \pm 0.53$	$0.44 \pm 0.02$	$136 \pm 2.1$	21	65	$6.86 \pm 0.69$	$4.77 \pm 0.48$	$0.56 \pm 0.02$
0223-0033	0.46	63	$7.78 \pm 0.78$	$0.26 \pm 0.03$	$176 \pm 3.4$	39	43	$12.98 \pm 1.40$	$5.19 \pm 0.56$	$0.57 \pm 0.02$
UGC5035	0.84	33	$13.78 \pm 1.38$	$0.44 \pm 0.01$	$77 \pm 1.3$	170	87	$16.43 \pm 1.64$	$11.86 \pm 1.19$	$0.53 \pm 0.01$
UGC9087	0.72	44	$19.15 \pm 1.91$	$0.54 \pm 0.02$	$28.5 \pm 2.0$	17	11.5	$19.50 \pm 1.95$	$6.81 \pm 0.68$	$0.39 \pm 0.03$
LSBCF568-08	0.78	39	$7.07 \pm 0.71$	$0.20 \pm 0.01$	$121 \pm 1.6$	63	58	$8.58 \pm 0.86$	$5.76 \pm 0.58$	$0.33 \pm 0.01$
LSBCF568-09	0.96	16	$12.53 \pm 1.25$	$0.39 \pm 0.01$	$60 \pm 1.1$	13	47	$12.80 \pm 1.28$	$6.90 \pm 0.69$	$0.40 \pm 0.01$
UGC9634	0.47	62	$10.36 \pm 1.04$	$0.63 \pm 0.01$	$89 \pm 0.5$	100	11	$10.98 \pm 1.10$	$9.00 \pm 0.90$	$0.35 \pm 0.01$
IC742	0.95	17	$16.68 \pm 1.67$	$0.64 \pm 0.01$	$117.6 \pm 0.7$	0	62.4	$17.28 \pm 1.73$	$7.53 \pm 0.75$	$0.65 \pm 0.01$
UGC8794	0.31	72	$11.39 \pm 1.14$	$0.48 \pm 0.01$	$42.1 \pm 0.8$	68	25.9	$19.05 \pm 1.93$	$10.78 \pm 1.09$	$0.63 \pm 0.01$
UGC9927	0.88	28	$13.78 \pm 1.38$	$0.42 \pm 0.01$	$109 \pm 0.8$	4	75	$15.49 \pm 1.55$	$4.49 \pm 0.45$	$0.48 \pm 0.01$
LSBCF584-01	0.75	41	$9.41 \pm 0.94$	$0.60 \pm 0.02$	$87 \pm 1.7$	76	11	$9.54 \pm 0.96$	$7.31 \pm 0.73$	$0.48 \pm 0.03$
LSBCF580-02	0.8	37	$4.83 \pm 0.48$	$0.57 \pm 0.03$	$115 \pm 2.0$	130	15	$4.92 \pm 0.49$	***	$0.48 \pm 0.04$
UGC3968	0.85	32	$16.68 \pm 1.67$	$0.63 \pm 0.02$	$136 \pm 1.1$	26	70	$19.34 \pm 1.93$	$8.53 \pm 0.85$	$0.68 \pm 0.01$
1300+0144	0.24	76	$7.07 \pm 0.71$	$0.63 \pm 0.01$	$82.6 \pm 0.7$	82	0.6	$7.08 \pm 0.71$	$5.63 \pm 0.56$	$0.35 \pm 0.02$
PGC60365	0.71	44	$9.41 \pm 0.94$	$0.41 \pm 0.02$	$169 \pm 1.9$	120	49	$11.64 \pm 1.17$	***	$0.49 \pm 0.02$
CGCG006-023	0.63	51	$8.56 \pm 0.86$	$0.37 \pm 0.01$	$30 \pm 1.3$	109	79	$13.44 \pm 1.34$	$10.02 \pm 1.00$	$0.60 \pm 0.01$
1252+0230	0.88	33	$7.07 \pm 0.71$	$0.29 \pm 0.03$	$88.3 \pm 3.1$	99	10.7	$7.12 \pm 0.71$	$6.57 \pm 0.66$	$0.18 \pm 0.03$
LSBCF570-01	0.60	53	$7.78 \pm 0.78$	$0.17 \pm 0.01$	$29 \pm 1.4$	108	79	$12.77 \pm 1.28$	$6.65 \pm 0.67$	$0.50 \pm 0.00$
1442+0137	0.9	26	$6.43 \pm 0.64$	$0.42 \pm 0.02$	$31 \pm 1.8$	8	23	$6.55 \pm 0.65$	$4.33 \pm 0.43$	$0.38 \pm 0.02$
LSBCF675-01	0.75	41	$6.43 \pm 0.64$	$0.57 \pm 0.02$	$79 \pm 1.8$	72	7	$6.47 \pm 0.65$	$4.39 \pm 0.44$	$0.44 \pm 0.03$
IC2423	0.81	36	$9.41 \pm 0.94$	$0.44 \pm 0.01$	$128 \pm 1.1$	100	28	$9.95 \pm 0.99$	$5.97 \pm 0.60$	$0.39 \pm 0.01$



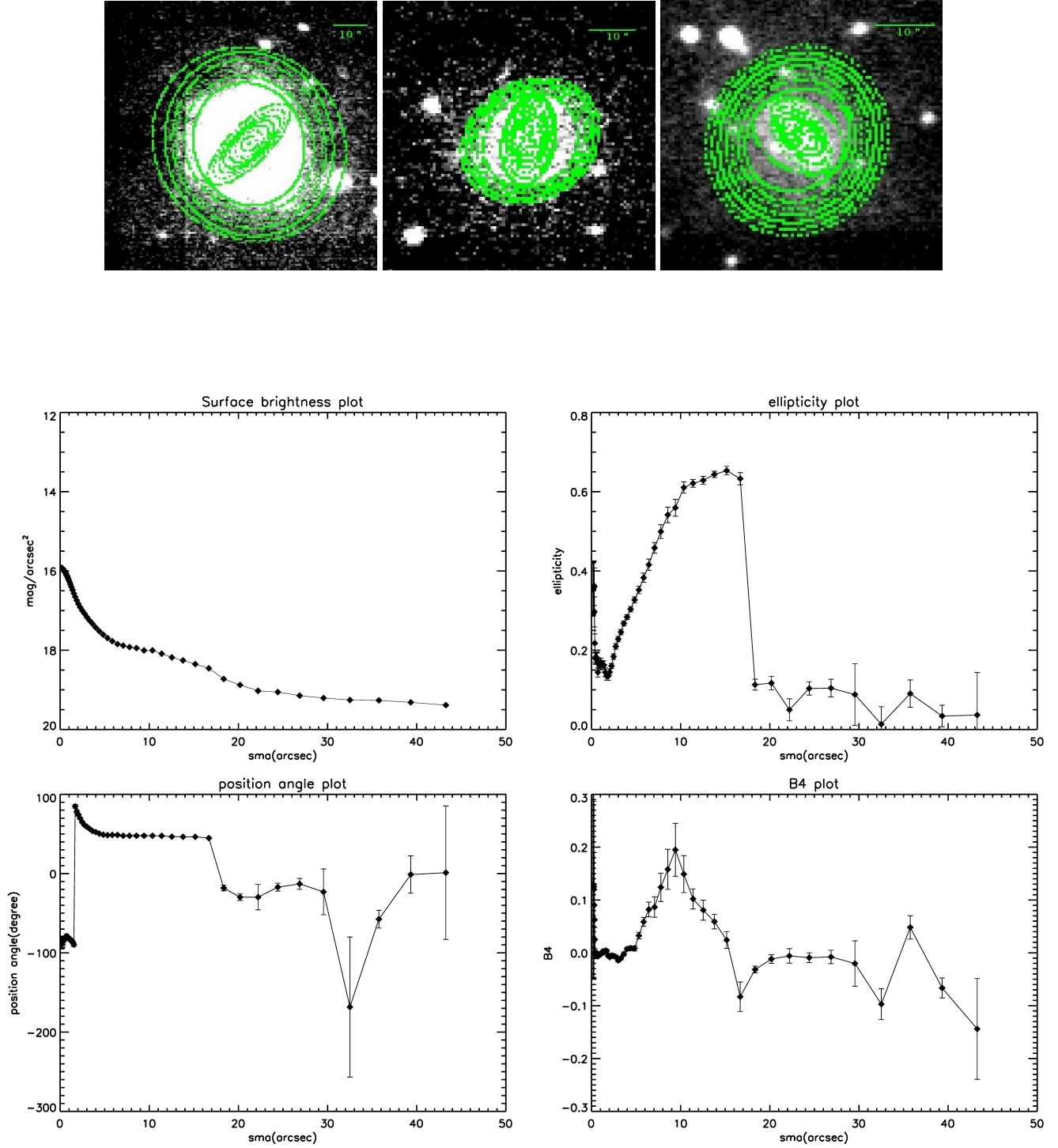
**Table 5.** The model magnitudes are taken from SDSS database for G-band and R-Band, which are used to determine the B-V color of the galaxy. The  $f_{\nu}$  represent the total flux in the R-band. For the calculations we have used the luminosity distance taken from NED. Lr, M/L and  $M_{stellar}$  denotes the R-band luminosity, the M/L ratio of the galaxy for that particular band and the stellar mass respectively.

Galaxy	g-r	B-V	$f_{\nu}$ (ergs cm <sup>-2</sup> s <sup>-1</sup> Hz)	Distance (Mpc)	Lr (ergs s <sup>-1</sup> Hz)	M/L	$M_{stellar}$ (10 <sup>10</sup> M <sub>⊙</sub> )
CGCG 381-048	0.629±0.003	0.836	8.47E-12	68.0	4.43E+42	2.78	0.62±0.01
UGC 1920	0.862±0.003	1.065	7.22E-12	83.4	5.68E+42	5.66	1.61±0.02
UGC 1455	0.889±0.002	1.091	2.60E-11	67.3	1.33E+43	6.14	4.09±0.03
NGC 5905	0.823±0.002	1.027	4.27E-11	47.8	1.10E+43	5.02	2.77±0.02
UM 163	0.728±0.003	0.933	1.25E-11	136.0	2.61E+43	3.76	4.89±0.04
UGC 11754	0.385±0.004	0.597	8.48E-12	62.5	3.75E+42	1.33	0.25±0.003
PGC 68495	0.633±0.004	0.840	5.40E-12	174.0	1.85E+43	2.82	2.61±0.03
UGC 2936	***	***	***	51.2	***	***	***
UGC 10405	0.651±0.004	0.858	7.60E-12	154.0	2.04E+43	2.98	3.03±0.03
0223-0033	0.990±0.003	1.191	2.03E-11	86.0	1.70E+43	8.35	7.11±0.07
UGC 5035	0.800±0.003	1.004	7.82E-12	161.0	2.29E+43	4.68	5.37±0.05
UGC 9087	0.939±0.003	1.140	1.41E-11	74.5	8.87E+42	7.15	3.17±0.03
LSBC F568-8	0.843±0.003	1.047	8.25E-12	148.0	2.04E+43	5.35	5.46±0.05
LSBC F568-9	0.682±0.003	0.888	6.97E-12	117.0	1.08E+43	3.27	1.76±0.02
UGC 9634	0.824±0.004	1.027	4.25E-12	184.0	1.63E+43	5.03	4.09±0.05
IC 742	0.934±0.003	1.135	8.69E-12	94.1	8.70E+42	7.04	3.06±0.03
UGC 8794	0.703±0.003	0.909	9.25E-12	124.0	1.61E+43	3.49	2.80±0.03
UGC 9927	0.772±0.003	0.976	1.52E-11	61.7	6.54E+42	4.30	1.41±0.01
LSBC F584-01	0.843±0.004	1.046	4.88E-12	171.0	1.61E+43	5.33	4.31±0.05
LSBC F580-2	0.608±0.004	0.816	5.52E-12	***	***	***	***
UGC 3968	0.722±0.003	0.928	1.17E-11	95.2	1.20E+43	3.69	2.21±0.02
1300+0144	0.730±0.005	0.935	2.99E-12	178.0	1.07E+43	3.78	2.03±0.03
PGC 60365	0.827±0.003	1.030	5.73E-12	***	***	***	***
CGCG 006-023	0.548±0.004	0.757	4.21E-12	166.0	1.31E+43	2.18	1.43±0.02
1252+0230	0.596±0.005	0.804	3.42E-12	209.0	1.69E+43	2.52	2.13±0.04
LSBC F570-01	0.812±0.003	1.016	8.93E-12	113.0	1.29E+43	4.86	3.13±0.03
1442+0137	0.587±0.005	0.795	2.74E-12	146.0	6.61E+42	2.45	0.81±0.01
LSBC F675-01	0.881±0.006	1.083	1.24E-12	150.0	3.15E+42	5.99	0.94±0.02
IC 2423	0.609±0.003	0.817	1.35E-11	132.0	2.65E+43	2.62	3.47±0.03

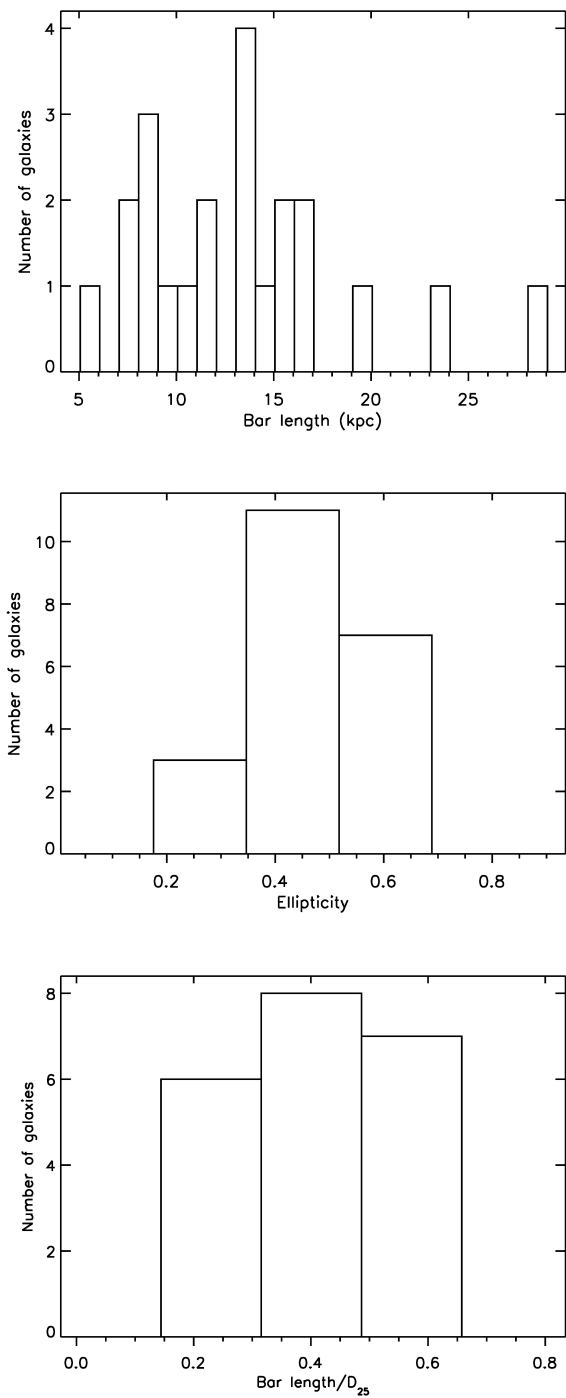
**Table 6.** The J and  $K_s$  values are taken from 2MASS extended object catalogue. J and  $K_s$  denotes the magnitudes in J and  $K_s$  bands. The HI values are taken from HYPERLEDA archival database. The columns m21,  $S_\nu$ ,  $M_{HI}$  are representing the HI magnitude, flux and the neutral hydrogen mass, that corresponds to the gaseous component of the galaxy.

Galaxy	J	$K_s$	m21	$S_\nu$ (Jy Km s <sup>-1</sup> )	$M_{HI}(10^9 M_\odot)$
CGCG 381-048	12.180±0.038	11.353 ±0.068	16.20±0.15	3.03 <sup>+0.45</sup> <sub>-0.39</sub>	3.30 <sup>+0.49</sup> <sub>-0.43</sub>
UGC 1920	12.273±0.038	11.081 ±0.051	15.56±0.12	5.45 <sup>+0.64</sup> <sub>-0.57</sub>	8.94 <sup>+1.04</sup> <sub>-0.94</sub>
UGC 1455	10.516±0.023	9.502 ±0.040	15.05±0.17	8.71 <sup>+1.26</sup> <sub>-1.48</sub>	9.31 <sup>+1.58</sup> <sub>-1.35</sub>
NGC 5905	10.467±0.017	9.514 ±0.027	13.61±0.12	32.8 <sup>+3.43</sup> <sub>-3.83</sub>	17.7 <sup>+2.07</sup> <sub>-1.85</sub>
UM 163	11.357±0.034	10.327 ±0.054	16.37±0.09	2.58 <sup>+0.21</sup> <sub>-0.22</sub>	11.3 <sup>+0.97</sup> <sub>-0.90</sub>
UGC 11754	12.823±0.075	11.853 ±0.106	15.06±0.13	8.63 <sup>+0.97</sup> <sub>-1.10</sub>	7.96 <sup>+1.01</sup> <sub>-0.90</sub>
PGC 68495	12.581±0.070	11.436 ±0.111	16.38±0.19	2.56 <sup>+0.41</sup> <sub>-0.49</sub>	18.3 <sup>+3.50</sup> <sub>-2.93</sub>
UGC 2936	10.160±0.026	8.914 ±0.029	14.97±0.14	9.38 <sup>+1.13</sup> <sub>-1.29</sub>	5.80 <sup>+0.80</sup> <sub>-0.70</sub>
UGC 10405	***	***	15.57±0.13	5.40 <sup>+0.61</sup> <sub>-0.69</sub>	30.20 <sup>+3.84</sup> <sub>-3.41</sub>
0223-0033	11.059±0.023	10.115 ±0.045	15.52±0.09	5.65 <sup>+0.45</sup> <sub>-0.49</sub>	9.86 <sup>+0.85</sup> <sub>-0.78</sub>
UGC 5035	12.168±0.040	11.144 ±0.049	***	***	***
UGC 9087	11.673±0.027	10.811 ±0.046	***	***	***
LSBC F568-8	12.232±0.061	11.177 ±0.072	***	***	***
LSBC F568-9	**	**	16.89±0.09	1.60 <sup>+0.13</sup> <sub>-0.14</sub>	5.17 <sup>+0.44</sup> <sub>-0.41</sub>
UGC 9634	12.761±0.044	12.068 ±0.084	15.84±0.22	4.22 <sup>+0.77</sup> <sub>-0.95</sub>	33.6 <sup>+7.55</sup> <sub>-6.17</sub>
IC 742	11.654±0.029	11.199 ±0.082	17.58±0.25	0.85 <sup>+0.17</sup> <sub>-0.22</sub>	1.77 <sup>+0.46</sup> <sub>-0.36</sub>
UGC 8794	11.893±0.028	10.893 ±0.039	16.41±0.15	2.49 <sup>+0.32</sup> <sub>-0.37</sub>	9.03 <sup>+1.34</sup> <sub>-1.17</sub>
UGC 9927	11.559±0.031	10.825 ±0.034	***	***	***
LSBC F584-01	12.551±0.041	11.844 ±0.079	17.26±0.16	1.14 <sup>+0.16</sup> <sub>-0.18</sub>	7.85 <sup>+1.25</sup> <sub>-1.08</sub>
LSBC F580-2	**	**	***	***	***
UGC 3968	12.100±0.039	11.073 ±0.059	15.79±0.12	4.41 <sup>+0.46</sup> <sub>-0.51</sub>	9.42 <sup>+1.10</sup> <sub>-0.99</sub>
1300+0144	13.044±0.058	12.158 ±0.106	16.92±0.27	1.56 <sup>+0.34</sup> <sub>-0.44</sub>	11.63 <sup>+3.28</sup> <sub>-2.56</sub>
PGC 60365	12.473±0.047	11.472 ±0.080	***	***	***
CGCG 006-023	13.286±0.068	12.378 ±0.116	***	***	***
1252+0230	13.698±0.083	12.752 ±0.145	***	***	***
LSBC F570-01	12.116±0.031	11.235 ±0.039	***	***	***
1442+0137	13.737±0.080	12.770 ±0.139	***	***	***
LSBC F675-01	13.954±0.066	13.294 ±0.148	16.91±0.42	1.57 <sup>+0.53</sup> <sub>-0.74</sub>	8.34 <sup>+3.94</sup> <sub>-2.68</sub>
IC 2423	11.811±0.028	10.866 ±0.044	16.47±0.42	2.36 <sup>+0.76</sup> <sub>-1.11</sub>	9.68 <sup>+4.57</sup> <sub>-3.11</sub>

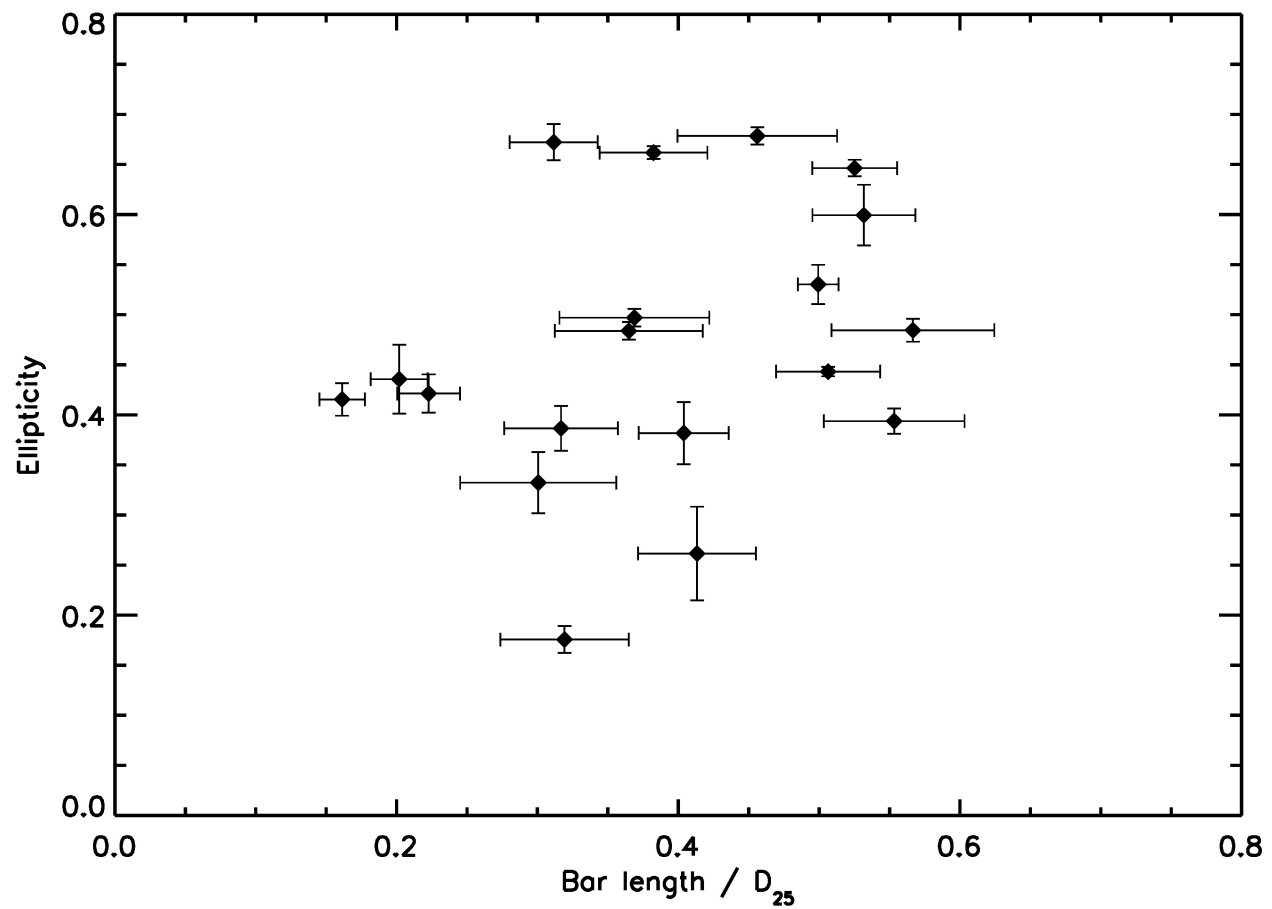
**Figure 4.** The fitted elliptical isophotes are overlaid on the Ks band image of galaxies UGC 3968, PGC60365 and UGC11754. Logscale is used in all images. The case of galaxy UGC 3968 is shown detailed with how the parameters like surface brightness, ellipticity, position angle and b4 parameter changes with the semi major axis



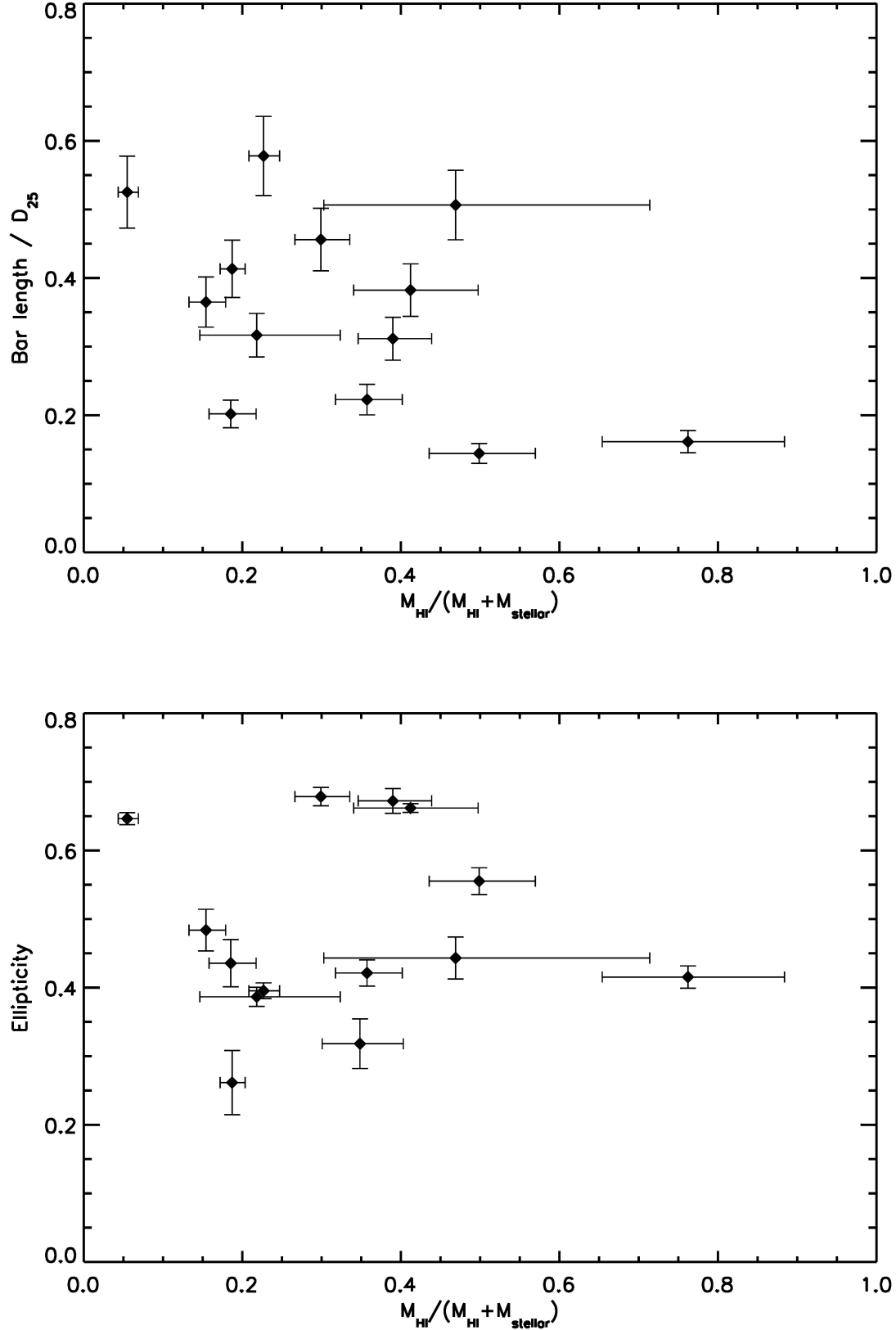
**Figure 5.** The histogram of deprojected barlength and deprojected ellipticities are shown below. The third figure show how the fraction of barlength to that of  $D_{25}$  is distributed

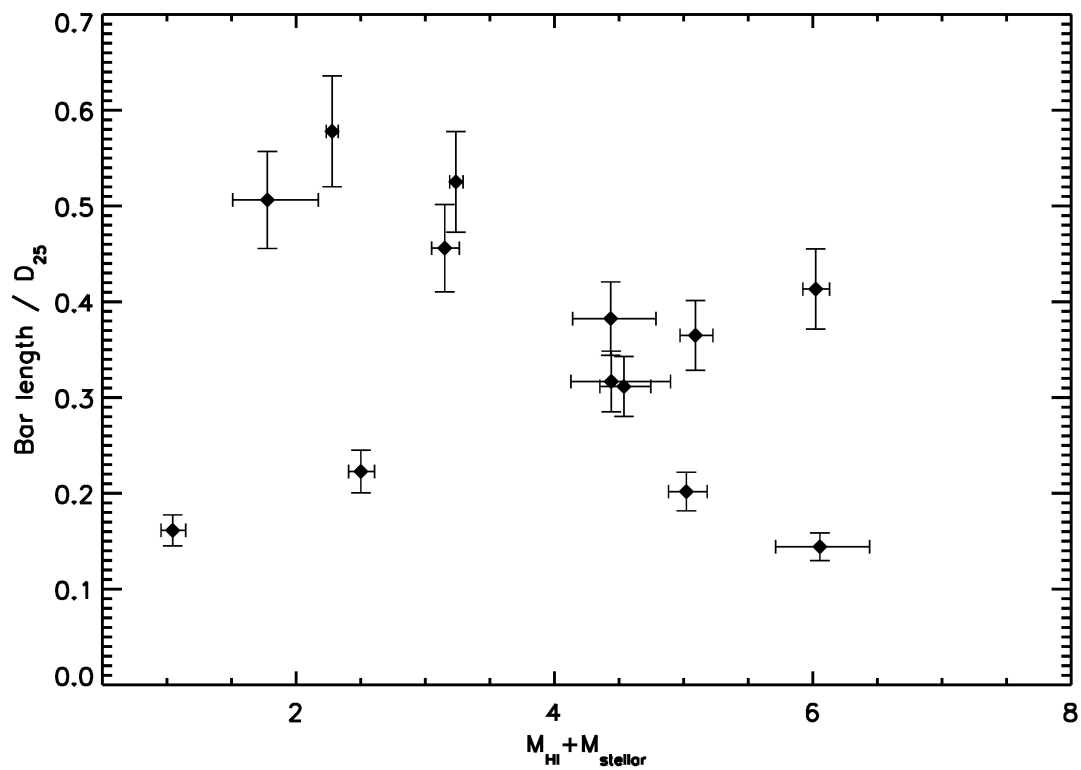


**Figure 6.** The ellipticity is plotted against the barlength to  $D_{25}$  parameter. The points are very scattered and not showing any correlation

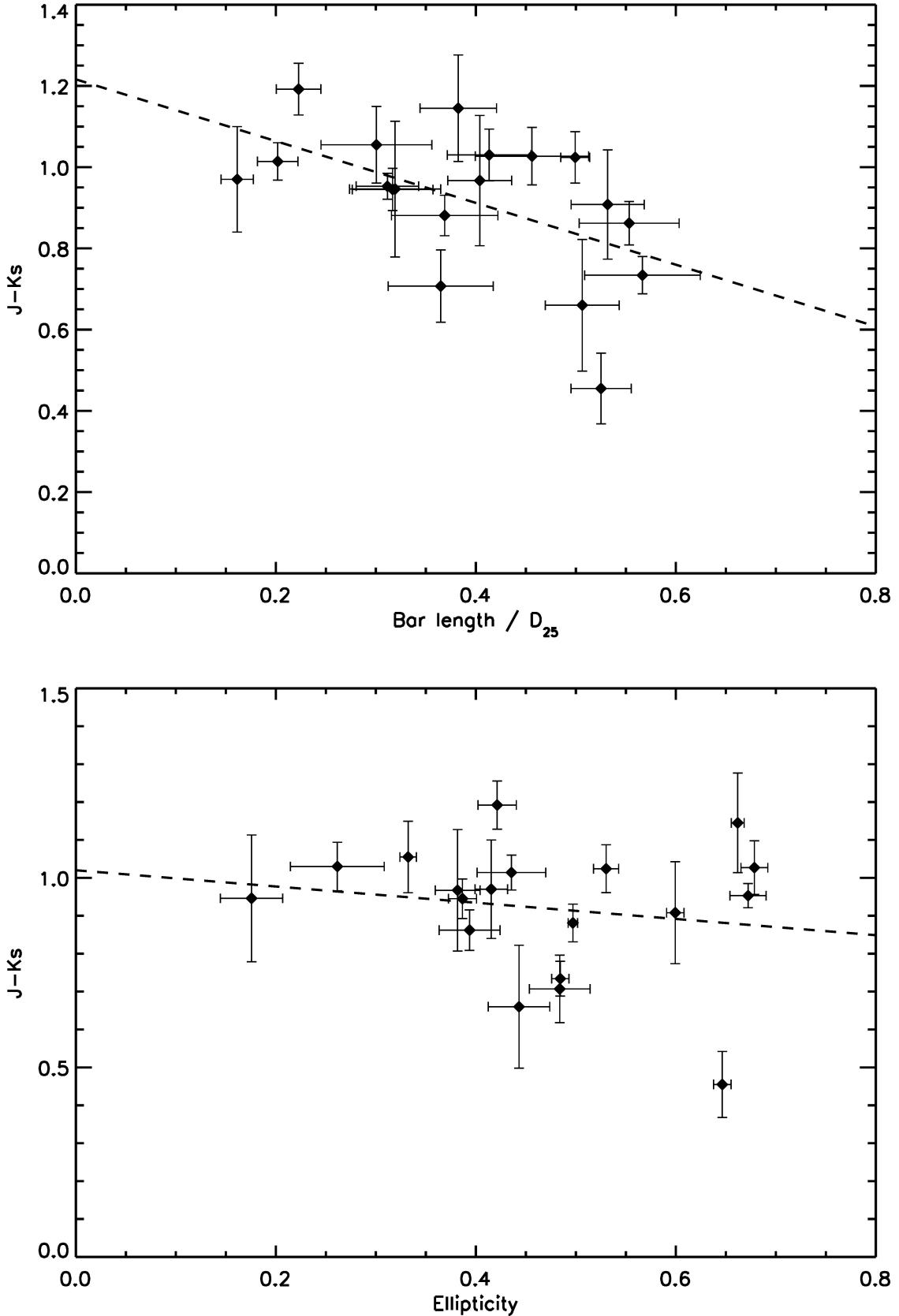


**Figure 7.** The bar parameters like barlength to  $D_{25}$  and ellipticity are plotted against the gas mass fraction of the galaxy. barlength to  $D_{25}$  and ellipticity are not showing any correlation with the  $M_{HI}$  to  $(M_{HI}+M_{stellar})$ , barlength to  $D_{25}$  to the total baryonic mass also scattered in nature.

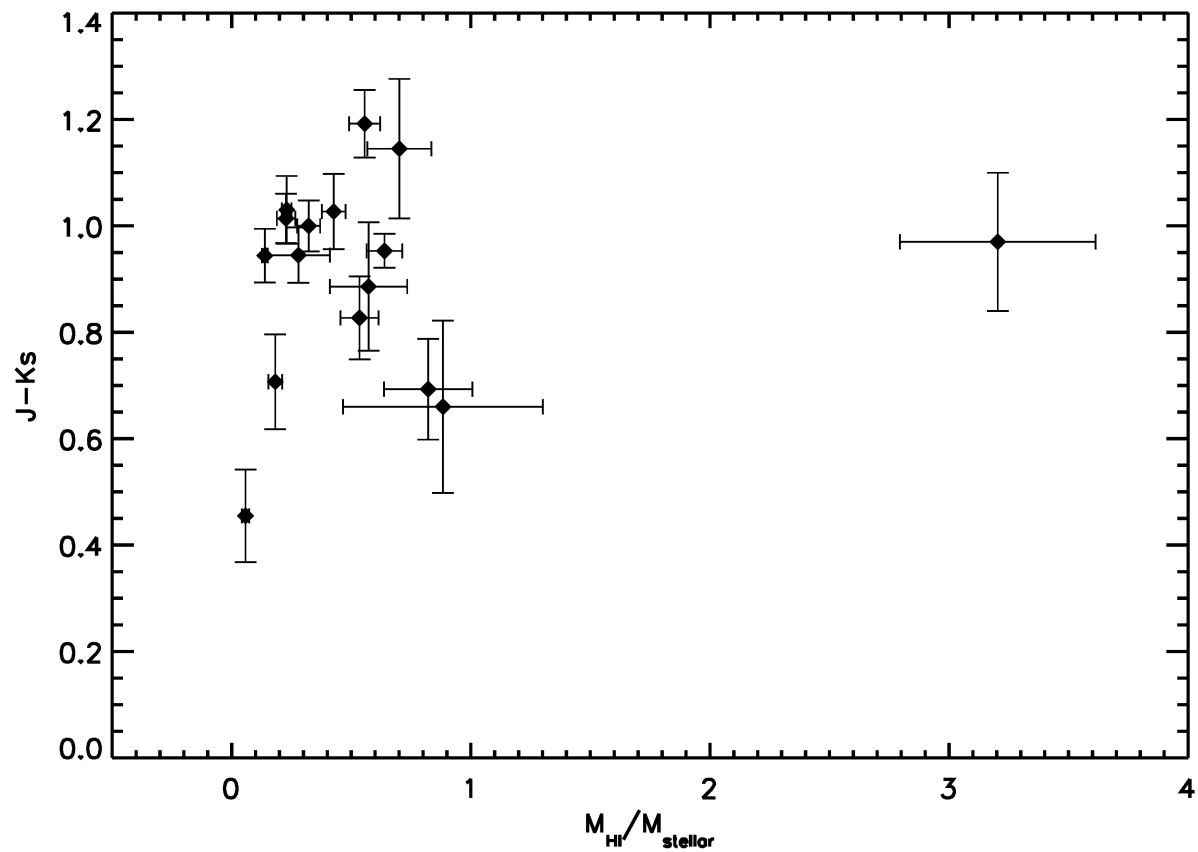




**Figure 8.** To check the variation of  $J-K_s$  with the bar parameters, we plotted the  $J-K_s$  against the ratio of barlength to  $D_{25}$  in the first plot and with ellipticity in the second plot. The ratio of barlength to  $D_{25}$  and ellipticity are showing a weak relation with the  $J-K_s$  color. The fitting does not include the errors





**Figure 9.** The J-K<sub>s</sub> color is plotted against the ratio of the gaseous mass to that of the stellar mass of the galaxy

## References

- Athanassoula E., 2002, *Astrophys. J. Lett.*, 569, L83
- Athanassoula E., 2003, *Mon. Not. Roy. Astron. Soc.*, 341, 1179
- Athanassoula E., Machado R. E. G., Rodionov S. A., 2013, *Mon. Not. Roy. Astron. Soc.*, 429, 1949
- Bell E. F., de Jong R. S., 2001, *Astrophys. J.*, 550, 212
- Boissier S. et al., 2008, *Astrophys. J.*, 681, 244
- Bournaud F., Combes F., Semelin B., 2005, *Mon. Not. Roy. Astron. Soc.*, 364, L18
- Buta R., 1986, *Astrophys. J. Suppl. Series*, 61, 609
- Chemin L., Hernandez O., 2009, *Astron. Astrophys.*, 499, L25
- Combes F., Debbasch F., Friedli D., Pfenniger D., 1990, *Astron. Astrophys.*, 233, 82
- Combes F., Sanders R. H., 1981, *Astron. Astrophys.*, 96, 164
- Das M., Anantharamaiah K. R., Yun M. S., 2001, *Astrophys. J.*, 549, 896
- Das M., Laurikainen E., Salo H., Buta R., 2008, *Astrophys. Spa. Sci.*, 317, 163
- Das M., O'Neil K., Vogel S. N., McGaugh S., 2006, *Astrophys. J.*, 651, 853
- Das M., Teuben P. J., Vogel S. N., Regan M. W., Sheth K., Harris A. I., Jefferys W. H., 2003, *Astrophys. J.*, 582, 190
- Davies J. I., Davies L. J. M., Keenan O. C., 2016, *Mon. Not. Roy. Astron. Soc.*, 456, 1607
- de Blok W. J. G., McGaugh S. S., Bosma A., Rubin V. C., 2001, *Astrophys. J. Lett.*, 552, L23
- Debatista V. P., Sellwood J. A., 1998, *Astrophys. J. Lett.*, 493, L5
- Efstathiou G., Lake G., Negroponte J., 1982, *Mon. Not. Roy. Astron. Soc.*, 199, 1069
- El-Zant A., Shlosman I., 2002, *Astrophys. J.*, 577, 626
- Ellison S. L., Nair P., Patton D. R., Scudder J. M., Mendel J. T., Simard L., 2011, *Mon. Not. Roy. Astron. Soc.*, 416, 2182
- Fanali R., Dotti M., Fiacconi D., Haardt F., 2015, *Mon. Not. Roy. Astron. Soc.*, 454, 3641
- Gadotti D. A., Athanassoula E., Carrasco L., Bosma A., de Souza R. E., Recillas E., 2007, *Mon. Not. Roy. Astron. Soc.*, 381, 943
- Galaz G., Dalcanton J. J., Infante L., Treister E., 2002, *Astronom. J.*, 124, 1360
- Heller C. H., Shlosman I., Athanassoula E., 2007, *Astrophys. J.*, 671, 226
- Hinz J. L., Rieke M. J., Rieke G. H., Willmer C. N. A., Misselt K., Engelbracht C. W., Blaylock M., Pickering T. E., 2007, *Astrophys. J.*, 663, 895
- Hoffman Y., Romano-Díaz E., Shlosman I., Heller C., 2007, *Astrophys. J.*, 671, 1108
- Hohl F., 1976, *Astronom. J.*, 81, 30
- Hunter J. D., 2007, *Computing In Science & Engineering*, 9, 90
- Impey C., Bothun G., 1997, *Annu. Rev. Astron. Astrophys.*, 35, 267
- Impey C. D., Sprayberry D., Irwin M. J., Bothun G. D., 1996, *Astrophys. J. Suppl. Series*, 105, 209
- Javanmardi B. et al., 2016, *Astron. Astrophys.*, 588, A89
- Jedrzejewski R. I., 1987, *Mon. Not. Roy. Astron. Soc.*, 226, 747
- Jester S. et al., 2005, *Astronom. J.*, 130, 873
- Kormendy J., Kennicutt, Jr. R. C., 2004, *Annu. Rev. Astron. Astrophys.*, 42, 603
- Long S., Shlosman I., Heller C., 2014, *Astrophys. J. Lett.*, 783, L18
- Makarov D., Prugniel P., Terekhova N., Courtois H., Vauglin I., 2014, *Astron. Astrophys.*, 570, A13
- Mapelli M., Moore B., 2008, *Astronomische Nachrichten*, 329, 948
- Marinova I., Jogee S., 2007, *Astrophys. J.*, 659, 1176
- Martin P., 1995, *Astronom. J.*, 109, 2428
- Martinez-Valpuesta I., Shlosman I., 2004, *Astrophys. J. Lett.*, 613, L29
- Martinez-Valpuesta I., Shlosman I., Heller C., 2006, *Astrophys. J.*, 637, 214
- Mayer L., Wadsley J., 2004, *Mon. Not. Roy. Astron. Soc.*, 347, 277
- McGaugh S. S., 1994, *Astrophys. J.*, 426, 135
- Menéndez-Delmestre K., Sheth K., Schinnerer E., Jarrett T. H., Scoville N. Z., 2007, *Astrophys. J.*, 657, 790
- Merritt A., van Dokkum P., Abraham R., 2014, *Astrophys. J. Lett.*, 787, L37
- Mihos J. C., McGaugh S. S., de Blok W. J. G., 1997, *Astrophys. J. Lett.*, 477, L79
- Mishra A., Kantharia N. G., Das M., Srivastava D. C., Vogel S. N., 2015, *Mon. Not. Roy. Astron. Soc.*, 447, 3649
- Ninan J. P. et al., 2014, *Journal of Astronomical Instrumentation*, 3, 50006
- Norman C. A., Sellwood J. A., Hasan H., 1996, *Astrophys. J.*, 462, 114
- O'Neil K., Bothun G., van Driel W., Monnier Ragaigne D., 2004, *Astron. Astrophys.*, 428, 823
- Ostriker J. P., Peebles P. J. E., 1973, *Astrophys. J.*, 186, 467
- Pickering T. E., Impey C. D., van Gorkom J. H., Bothun G. D., 1997, *Astronom. J.*, 114, 1858
- Pickering T. E., van Gorkom J. H., Impey C. D., Quillen A. C., 1999, *Astronom. J.*, 118, 765
- Pustilnik S. A., Martin J.-M., Tepliakova A. L., Kniazev A. Y., 2011, *Mon. Not. Roy. Astron. Soc.*, 417, 1335
- Raha N., Sellwood J. A., James R. A., Kahn F. D., 1991, *Nature*, 352, 411
- Rahman N., Howell J. H., Helou G., Mazzarella J. M., Buckalew B., 2007, *Astrophys. J.*, 663, 908
- Renaud F. et al., 2015, *Mon. Not. Roy. Astron. Soc.*, 454, 3299
- Roberts M. S., 1975, *Radio Observations of Neutral Hydrogen in Galaxies*, Sandage A., Sandage M., Kristian J., eds., the University of Chicago Press, p. 309
- Rosenbaum S. D., Krusch E., Bomans D. J., Dettmar R.-J., 2009, *Astron. Astrophys.*, 504, 807
- Saha K., Naab T., 2013a, *Mon. Not. Roy. Astron. Soc.*, 434, 1287
- Saha K., Naab T., 2013b, *Mon. Not. Roy. Astron. Soc.*, 434, 1287
- Schombert J., 1998, *Astronom. J.*, 116, 1650
- Schombert J. M., Bothun G. D., 1988, *Astronom. J.*, 95, 1389
- Schombert J. M., Bothun G. D., Schneider S. E., McGaugh S. S., 1992, *Astronom. J.*, 103, 1107

- Sellwood J. A., Wilkinson A., 1993, Reports on Progress in Physics, 56, 173
- Sheth K., Vogel S. N., Regan M. W., Thornley M. D., Teuben P. J., 2005, *Astrophys. J.*, 632, 217
- Simmons B. D. et al., 2014, *Mon. Not. Roy. Astron. Soc.*, 445, 3466
- Skrutskie M. F. et al., 2006, *Astronom. J.*, 131, 1163
- Sormani M. C., Binney J., Magorrian J., 2015, *Mon. Not. Roy. Astron. Soc.*, 449, 2421
- Sprayberry D., Impey C. D., Bothun G. D., Irwin M. J., 1995, *Astronom. J.*, 109, 558
- Villa-Vargas J., Shlosman I., Heller C., 2009, *Astrophys. J.*, 707, 218
- Villa-Vargas J., Shlosman I., Heller C., 2010, *Astrophys. J.*, 719, 1470
- Weinberg M. D., 1985, *Mon. Not. Roy. Astron. Soc.*, 213, 451
- Zou Y., Shen J., Li Z.-Y., 2014, *Astrophys. J.*, 791, 11